J. Fluid Mech. (2022), *vol*. 951, A46, doi:10.1017/jfm.2022.883

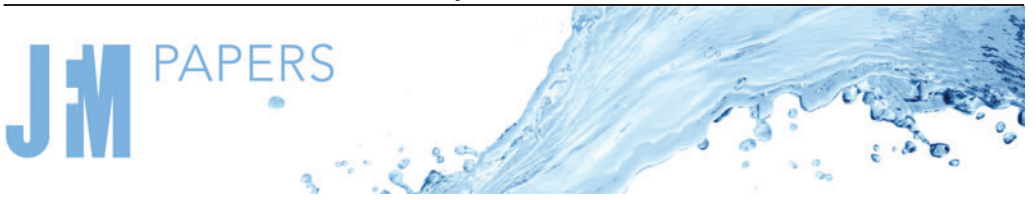

A comparative study of experiments with numerical simulations of free-stream turbulence transition

Santhosh B. Mamidala[1], **André Weingärtner**[1] **and Jens H.M. Fransson**[1],†

[1]KTH Engineering Mechanics, Teknikringen 8, 114 28 Stockholm, Sweden

(Received 4 July 2022; revised 5 September 2022; accepted 11 October 2022)

To date, very few careful and direct comparisons between experiments and direct numerical simulations (DNS) have been published on free-stream turbulence (FST) induced boundary layer transition, whilst there exist numerous published works on the comparison of canonical turbulent boundary layers. The primary reason is that the former comparison is vastly more difficult to carry out simply because all known transition scenarios have large energy gradients and are extremely sensitive to surrounding conditions. This paper presents a detailed comparison between new experiments and available DNS data of the complex FST transition scenario in a flat plate boundary layer at turbulence intensity level about $Tu = 3\,\%$ and FST Reynolds number about $Re_{fst} = 67$. The leading edge (LE) pressure gradient distribution and the full energy spectrum at the LE are identified as the two most important parameters for a satisfying comparison. Matching the LE characteristic FST parameters is not enough as previously thought, which is illustrated by setting up two experimental FST cases with about the same FST integral parameters at the LE but with different energy spectra. Finally, an FST boundary layer penetration depth (PD) measure is defined using DNS, which suggests that the PD grows with the downstream distance and stays around 20 % of the boundary layer thickness down to transition onset. With this result, one cannot rule out the significance of the continuous FST forcing along the boundary layer edge in this transition scenario, as indicated in previous studies.

Key words: boundary layer receptivity, boundary layer stability, transition to turbulence

† Email address for correspondence: jensf@kth.se

1. Introduction

Through the years, a theoretical framework has been established in laminar–turbulent boundary layer (BL) transition through the observed phenomena from both experiments and simulations. The most complex transition scenario, undeniably the one induced by free-stream turbulence (FST), has eluded researchers over several decades. From the existing literature, it is clear that for the FST induced BL transition scenario in its very simplest case, i.e. for a zero pressure gradient flow, researchers are still raising questions on the receptivity process, and it seems that consensus is not reached on the breakdown process of unsteady streamwise streaks into turbulent spots when originating from FST. For a long time, the turbulence intensity in the free stream (Tu) was used as a single parameter to predict the transitional Reynolds number, but as more well-documented data have become available, the community has understood that this transition scenario is far more complicated to comprehend. Several experiments or direct numerical simulations (DNS) with seemingly similar conditions can have a widespread disagreement in results regarding both the location and extent of transition. In experiments, this can be due to multitude of parameters like small variations in Tu ($= u_{rms}/U_\infty$), differences in FST length scales, or different leading edge (LE) pressure gradients, but possibly also due to the FST condition in terms of inhomogeneity and anisotropy, just to mention some parameters of importance. Here, u_{rms} corresponds to the root-mean-square (r.m.s.) of the streamwise velocity component, and U_∞ corresponds to the mean free-stream velocity. Direct comparisons between experiments and DNS are therefore important for two reasons. First, the two approaches are frequently used for validation of model-based computational fluid dynamics (CFD), where mathematical models describe complex fluid physics. This type of validation is redundant unless one can certify that detailed results from experiments with DNS or vice versa can be reproduced. Second, a direct comparison may pinpoint the critical parameters that are important to match for a satisfying comparison and hence can give guidance on how to develop better CFD models.

The following introduction is not intended to give a complete account of the FST transition scenario; instead, interested readers are referred to the experimental works by e.g. Matsubara & Alfredsson (2001) or Fransson & Shahinfar (2020). However, some results significant for the later comparisons in the present paper are summarized below.

The first FST BL measurements of streamwise disturbance growth were performed by Klebanoff and are reported in Kendall (1998). Here, it is shown that the maximum u_{rms} inside the BL grows as the square root of the downstream distance. About the same time, Arnal & Juillen (1978) also reported streamwise BL disturbance growth reaching several per cent of U_∞ prior to breakdown to turbulence. These results were confirmed in Westin *et al.* (1994), where the maximum disturbance level inside the BL was reported to reach around 10 % with only a minor modulation of the mean velocity BL profile. Additional experiments supporting the disturbance growth were reported by Matsubara & Alfredsson (2001), who demonstrated that for flat plate Reynolds number $Re_x < 10^5$, the disturbance energy $E = u_{rms}^2/U_\infty^2$ is proportional to Re_x in the initial region close to the LE ($Re_x = xv/U_\infty$). Later, Fransson, Matsubara & Alfredsson (2005), in agreement with Andersson, Berggren & Henningson (1999), showed using many different turbulence generating grids that the energy is proportional to both Tu^2 and Re_x. Fransson *et al.* (2005) studied this transition scenario under an extensive range of Tu and length scales, but did not organize their data according to integral length scales. However, it was hypothesized that in the receptivity process transpiring at the LE initially, FST scales require a distance to adjust to the BL.

Today, it is not new to claim that the FST integral length scale Λ_x is important for the transition process. As pointed out by Fransson & Shahinfar (2020), already in the results by Hislop (1940) one can discern an effect of the mesh width (M) on the transitional Reynolds number (Re_{tr}). It is noteworthy that $\Lambda_x \sim \sqrt{M}$ (see e.g. Kurian & Fransson 2009) and that the Hislop (1940) results indicate that transition moves downstream with increasing M. Later works, both experiments and DNS, showed the opposite effect, i.e. that transition moved upstream with increasing Λ_x (see Jonáš, Mazur & Uruba 2000; Brandt, Schlatter & Henningson 2004, respectively). The latter trend was believed to be the true effect of Λ_x on Re_{tr} until both trends were captured in the same experimental set-up by Fransson & Shahinfar (2020), who explain the phenomenon by scale-matching, and their nonlinear model is shown to capture the twofold effect seemingly well.

In many well-known DNS studies on FST induced transition (e.g. Jacobs & Durbin 2001; Brandt *et al.* 2004), the LE is not present, either because of the used numerical code with limitations of handling complex geometries or to reduce the computational costs but possibly also due to lacking perceptions on LE receptivity at the time. However, in most real flow applications, an LE is present, and the effect of the LE pressure gradient was brought up already by Westin *et al.* (1994) as a possible parameter influencing Re_{tr}, with a focus on the LE shape factor. In their figure 15, they compare the downstream development of shape factors from different experiments and associate high values of LE shape factors (i.e. strong LE pressure suction peaks) with earlier transition even though none of the experiments had similar FST conditions. However, in a recent study by Mamidala, Weingärtner & Fransson (2022), the LE pressure gradient, quantified by the Falkner–Skan BL parameter (m), was varied systematically in a set-up where Tu and Λ_x could be varied independent of each other. Their data showed up to 40 % variation in Re_{tr} for their studied m range under constant Tu, and were shown to be most sensitive for small Λ_x.

Apart from correlating Re_{tr} to the LE FST characteristics, the free-stream turbulence penetrating the BL edge along the downstream streamwise distance could be an essential continuous path of receptivity. Early speculations by Dyban, Epik & Suprun (1976) argue that there are two events: (1) penetration of FST into the BL; (2) generation of disturbances within the BL itself. These mechanisms both contribute to the modulation of the developing BL in the presence of FST. Starting with penetration (1), Jacobs & Durbin (1998) proposed the 'shear-sheltering' concept assuming that FST consists of a superposition of continuous modes. Continuous modes that oscillate in the free-stream damp rapidly inside the BL, and they are expelled out of the sheared region unless their frequency is low (Grosch & Salwen 1978; Bertolotti 1997). Low-frequency disturbances have the ability to penetrate the BL, which is often called shear sheltering. Later, Hunt & Durbin (1999) presented a rationale for the low-frequency part of FST broadband entering the BL. This concept was, however, already observed in the experiments by Westin (1997), who stated that the BL acts as a 'low-pass filtered amplifier' for FST. Systematic studies have later verified this concept and brought additional insights (see e.g. Zaki & Durbin 2005; Zaki & Saha 2009; Wang, Mao & Zaki 2019). The disturbance growth inside the BL (2) is characterized by algebraic growth of unsteady streamwise velocity streaks, which is explained by the lift-up mechanism (Ellingsen & Palm 1975; Landahl 1980; Hultgren & Gustavsson 1981). Now, considering that the BL develops over a hydrodynamically smooth surface, the exchange of momentum will be initiated by a vertical motion towards the wall by the FST forcing, which leads to low-momentum fluid being lifted from the wall due to continuity. This means that (1) and (2) are coupled, and that (1) is the driver and (2) is the driven event.

Despite these expectedly coupled events, (1) and (2), there is still a current issue of whether the importance of the FST forcing is limited to the LE region or if it is persistent and plays an important role as a driver even far downstream. A question that has often been asked in the literature is: 'Do free-stream perturbations couple to boundary layer perturbations at receptivity sites, or do they penetrate continuously into the developing boundary layer?' (Durbin 2017). In order to answer this, one needs to quantify the magnitude for depth of the penetration of FST into the BL. Note that in the literature, there is no uniform definition for penetration depth. First ideas of Dyban *et al.* (1976), choosing u_{rms}^{max} as a measure of penetration depth, seem inappropriate because u_{rms}^{max} can exist inside the BL even without FST, for example in the velocity fluctuations of Taylor (1939) (see figure 10) or optimal growth of Andersson *et al.* (1999) and Luchini (2000). For continuous modes, Jacobs & Durbin (1998) show that for an assumed piecewise linear velocity profile, penetration depth δ scales as $\tau^{1/3}\delta \propto (\omega R)^{-1/3}$, where δ is defined from the BL edge, τ is the shear stress, R is the Reynolds number based on the BL thickness, and ω is the frequency. However, for a Blasius BL, it scales as $\delta \propto (\omega R)^{-0.133}$ and $\delta \propto \tau^{-4.5}$ (Jacobs 2000, for detailed information, see). All these rationales are jotted down based on the definition that δ is the distance below the BL edge where the eigenfunctions (magnitude of perturbations $\sim u_{rms}$) dropped below 0.01. Later, Maslowe & Spiteri (2001) defined the distance from the BL edge to the first maximum eigenfunction close to the wall as δ. However, Zaki & Durbin (2005) demonstrated that the aforementioned usage of penetration depth, as such, is not an ideal measure of the effectiveness of disturbances penetrating the BL. Zaki & Saha (2009) integrated the eigenfunction (normalized by its free-stream value) up to the BL edge to obtain penetration depth. Their penetration depth scaled with k_xR (where $k_x = \omega/U_\infty$ is the wavenumber), and it decreases abruptly when the parameter k_xR is large.

First experimental validation for the definition of penetration depth (PD) by Jacobs & Durbin (1998) was provided in Hernon, Walsh & McEligot (2007). The tested correlation was slightly different as $PD \propto (\omega\, Re_x\, \tau_w)^{-0.3}$. They defined penetration depth as the distance from the BL edge to the skewness maximum, and used $\omega = U_\infty/\Lambda_x$, corresponding to the frequency of largest eddies in the free-stream, and τ_w, i.e. the wall-shear stress instead of the local τ. However, they conclude that their proposed correlation is accurate only to within $\pm 50\,\%$, which can be considered poor. Here, it should be pointed out that the location of peak skewness is truly a statistical parameter like u_{rms}^{max} and again is not appropriate for defining the penetration depth since the wall-normal location of peak skewness seems to be already at the BL edge and gradually moves out of the BL (as observed in Kalfas 1994; Mamidala 2022).

Subsequently, Nolan & Walsh (2012) performed high-speed particle image velocimetry measurements in transitional BLs and investigated penetration depth from a different point of view, namely through two-point spatial correlations of streamwise C_{uu} and wall-normal C_{vv} fluctuations. They conclude that the measure C_{uu}, where the effect of FST should define the penetration depth, is contaminated by the streamwise streaks inside the BL. However, they also conclude that for C_{vv}, where the u'-dependent streaks on the correlation coefficient are minimized gives a relatively poor correlation across the BL edge until the first appearance of turbulent spots at the wall. Their overall conclusion is that FST does not penetrate the BL noticeably.

In the present paper, an initiative is taken to use an available DNS database (Zaki 2013) and try to replicate the results in a new experiment, denoted EXP1, in order to

identify the most important factors for the FST transition process, and to answer some of the questions raised in this introduction. In addition, two more experimental cases are presented, EXP2 and EXP3, by varying Λ_x while keeping Tu constant, and an additional experimental case, EXP4, seemingly close to the EXP1 case when comparing the LE characteristic FST parameters but with a very different LE FST energy spectrum. The aim of the current investigation is to gain further insight into BL transition caused by FST, i.e. not only to match previous DNS results, but to obtain a better understanding of the sensitivity to external conditions. The current work begins in § 2 with a brief outline of the experimental set-up, accompanied by measurement techniques, an overview on the basis of the comparative study with DNS, and an account of the procedure of calculating the intermittency factor. In § 3, the experimental matching of base conditions with DNS is shown. This is followed in § 4 by the data analyses, and experimental results of EXP1 premised on a matching case with DNS, certain essential criteria in FST experiments, and BL statistics. In § 5, the BL receptivity is addressed in terms of the sensitivity to the LE energy spectrum and the FST penetration depth. The paper ends with a discussion and conclusions in § 6.

2. Experimental set-up and methods

2.1. *Experimental facility*

The present experimental investigation was carried out in the closed-circuit type minimum turbulence level (MTL) wind tunnel situated at KTH Royal Institute of Technology in Stockholm. This low-speed tunnel has a working section 7 m in length with cross-sectional area $1.2 \times 0.8\,\mathrm{m}^2$. The tunnel provides a maximum speed $70\,\mathrm{m\,s}^{-1}$ in an empty test section. The free-stream turbulence intensity is lower than 0.025 % in the streamwise direction at a nominal speed $25\,\mathrm{m\,s}^{-1}$. The inbuilt PID controller system linked to the heat exchanger can control the air temperature within $\pm 0.05\,^{\circ}\mathrm{C}$ inside the working section (Lindgren & Johansson 2002, for more information, cf.).

Measurements were conducted on a flat plate 4.2 m in length with a 160 mm long asymmetric LE (see figure 1). The LE is 20 mm thick and is designed to produce a minimal LE pressure gradient region. This LE was first used in the experimental work of Klingmann *et al.* (1993) and later in the FST investigations of Matsubara & Alfredsson (2001), Fransson *et al.* (2005) and Fransson & Shahinfar (2020). The compliant ceiling of the test section is used to adjust the pressure gradient on the test plate. A 450 mm long trailing edge flap was added downstream of the flat plate in order to tune the position of the stagnation line at the LE.

Four turbulence generating grids were used in the present experiments to tailor different FST conditions at the LE, namely the FST intensity ($Tu = u_{rms}/U_\infty$) and the FST integral length scale (Λ_x). Each grid was mounted upstream of the LE with a relative distance x_{grid} between the grid and the LE to generate the test cases studied. The grids are characterized by their mesh width M, bar diameter d, and solidity $\sigma = d/M(2 - d/M)$ (the grids used in this study have the same solidity of 0.36). In all the cases, the grids are placed at least 20 mesh widths upstream of the LE in order to allow the generated turbulence to be homogeneous with a low level of anisotropy at the LE. Twenty mesh widths are often used as a rule of thumb for a minimum distance to accomplish homogeneous turbulence, but this can be longer for some grids. The different grids are summarized in table 1.

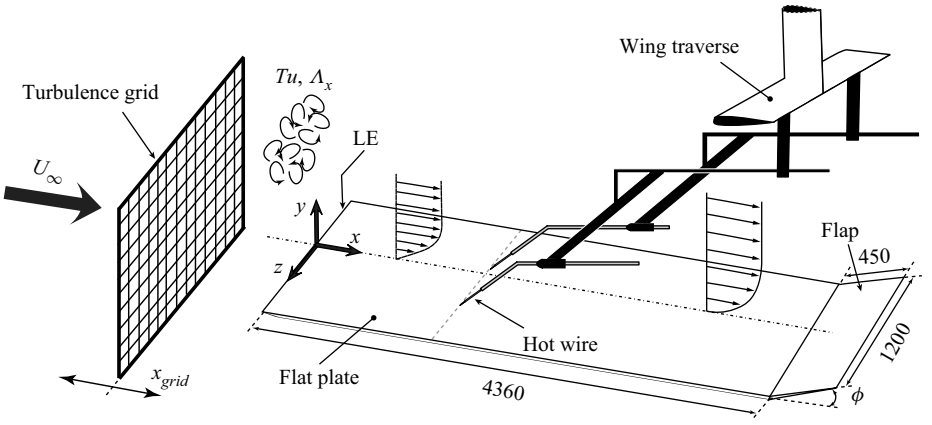

Figure 1. Brief schematic of the experimental set-up (dimensions are in mm).

Case	Grid	M (mm)	d (mm)	x_{grid} (mm)	Tu (%)	Λ_x (mm)	Re_Λ	Re_{fst}	x_{tr} (mm)	Re_{tr}	$\lambda_{z,on}$ (mm)
DNS	—	—	—	—	3.12	5.32	2153	67	620	250 480	8.64
EXP1	G0	10	2	270	3.13	5.31	2152	67	624	249 440	8.76
EXP2	G17	40	8	890	3.12	14.75	5938	185	481	193 649	10.95
EXP3	G19	50	10	2300	3.14	28.84	11 610	364	465	187 087	11.74
EXP4	G15	6	1.2	137	3.00	4.81	1874	57	1792	698 182	7.87

Table 1. Grid data, FST conditions at the LE, and transition parameters. The grid numbers G17, G19 and G15 are similar to those in Fransson & Shahinfar (2020). Note that in DNS, the values at the LE are extrapolated.

2.2. *Measurements and instrumentation*

A DANTEC Dynamics anemometer system (Streamline CTA 90N10 Frame – 90C10 modules) coupled with an NI 6215 DAQ system was used for hot-wire data acquisition. In this study, the signals were acquired for a sampling time of 120 s with sampling frequency 20 kHz. The hot-wire probes were calibrated *in situ* against a Prandtl tube by placing them at the same streamwise location in the free stream. The dynamic pressure values obtained from the Prandtl tube and the ambient conditions were read through a differential manometer (Furness FCO560).

Experiments include both free-stream and BL measurements using a dual-probe set-up with two hot-wire probes. The probes are mounted on a wing traverse facilitating the streamwise, wall-normal and spanwise measurements, with one probe being traversable in the spanwise direction relative to the other (as shown with Cartesian coordinates x, y, z, respectively, in figure 1). Single-point velocity measurements, transition location, and two-point correlation measurements were performed inside the BL.

2.3. *Comparative study with DNS*

The transitional BL data produced from DNS of Zaki (2013) over a flat plate with an elliptic LE can be accessed openly through the Johns Hopkins Turbulence Database (JHTDB 2021*b*). The present experiment EXP1 has been designed to match this DNS flow case by tuning the LE pressure gradient and the FST conditions. In the simulations,

the inflow is perturbed by synthetic turbulence introduced in the form of Fourier modes in a periodic domain. Detailed information on the simulation domain, inflow, discretization algorithm and data stored can be found in the dataset description (JHTDB 2021*a*) on the JHTDB site.

In the DNS, the reference length scale is L_{ref}, which is specified to be the half-thickness of the plate. The Reynolds number based on the non-dimensional inflow parameters $L_s = 1$ (length scale) and $U_s = 1$ (velocity scale) is $Re_{L,s} = U_s L_s/\nu_s = 800$, giving a non-dimensional kinematic viscosity $\nu_s = 1.25 \times 10^{-3}$. The data stored on the JHTDB site are available in the streamwise range $x_s = x/L_{ref} = 30.2$–1000. The values of the streamwise integral length scale and turbulence intensity extrapolated at the LE position, i.e. at $x_s = 0$, are $\Lambda_{x,s} = \Lambda_x/L_{ref} = 2.66$ and $Tu_s = 3.12\,\%$, respectively. Now, in order to design an experimental case that matches the DNS, the following points should be addressed: (1) choice of speed in experiments; (2) matching the LE pressure distribution (cf. § 3.1); (3) choice of the turbulence generating grid that produces the same energy spectrum at the LE (cf. § 3.2); (4) securing that the experimental Reynolds number matches $Re_{L,s}$. Point (3) is not so easy to match experimentally, but as will be shown later in the paper, it is essential in order to obtain the same BL receptivity. This matching will not only guarantee the same Tu and Λ_x at the LE, it will also produce the same turbulence intensity decay and growth of the integral length scale in the free stream.

Let us consider the reference experimental condition for the velocity scale U_{ref} and length scale L_{ref}, choices that will decide the experimental dimensional condition as $U = U_s U_{ref}$, $L = L_s L_{ref}$ and $\nu = \nu_s L_{ref} U_{ref}$. From here, a reasonable velocity has to be chosen that can be changed for final tuning since it will not affect the experimental Tu or Λ_x. For a velocity $U_{ref} = 6.2\,\mathrm{m\,s^{-1}}$, which corresponds to a tuned value is a reasonable speed for transition experiments in the MTL wind tunnel, the velocity in the experiments then simply becomes $U = 6.2\,\mathrm{m\,s^{-1}}$. The choice will produce a relatively thick BL that can be spatially well-resolved without any effort, and the length of the plate in the tunnel is relatively long such that high enough Reynolds numbers can be obtained. This allows having a turbulent BL at the end of the measurement domain. With grid G0 (see table 1), the FST condition at the LE position corresponds to $Tu = 3.13\,\%$ and $\Lambda_x = 5.31\,\mathrm{mm}$. As a direct consequence of integral length scale-matching, the conversion factor for lengths between DNS and experiments becomes $L = L_{ref} = \Lambda_x/\Lambda_{x,s} = 2\,\mathrm{mm}$. With this choice, the Reynolds number based on L and U can be calculated as $Re_L = UL/\nu \approx 805$, which is close to the DNS value of $Re_{L,s}$. The kinematic viscosity in EXP1 was $\nu = 1.541 \times 10^{-5}\,\mathrm{m^2\,s^{-1}}$, which is a constant set by the atmospheric conditions inside the test section of the wind tunnel, used in calculating Re_L. The kinematic viscosities for EXP2, EXP3, EXP4 were $\nu = 1.562 \times 10^{-5}$, 1.538×10^{-5}, $1.553 \times 10^{-5}\,\mathrm{m^2\,s^{-1}}$, respectively.

2.4. *Intermittency detection method*

The location and extent of transition can be characterized using a quantity known as the intermittency factor (γ). This parameter describes the state of the flow, i.e. the amount of time for which the flow remains turbulent. A value of zero indicates fully laminar flow, while a value of unity implies fully turbulent flow. The long-established conditional sampling approach (Antonia & Bradshaw 1971; Hedley & Keffer 1974; Muck 1980) facilitates drawing a distinction between laminar/turbulent states using the factor γ. This sequential approach consists of four critical steps: (1) choice of detector function $\mathcal{D}(t)$ to sensitize the turbulent signatures; (2) choice of criterion function $\mathcal{C}(t)$ to emphasize high-frequency components; (3) determining the adaptive threshold level $\mathcal{C}^{th}$;

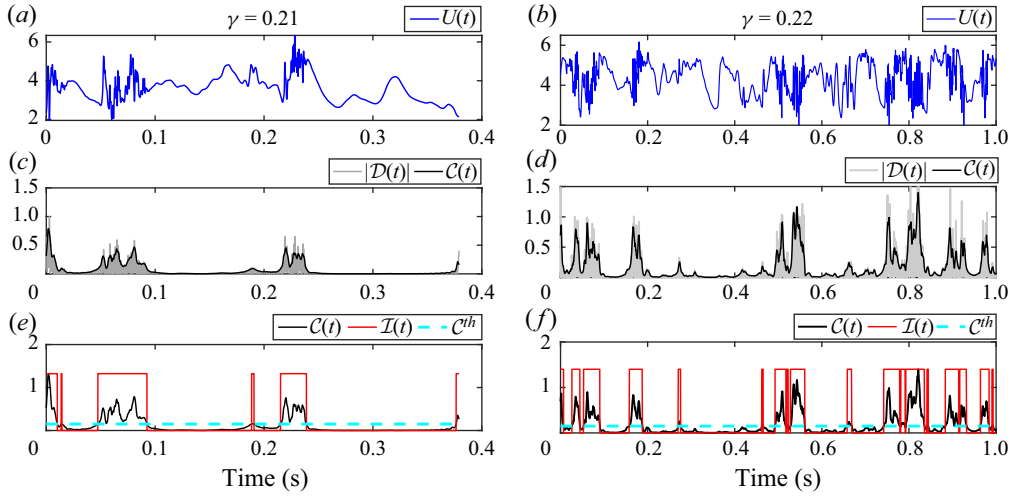

Figure 2. Illustration of the intermittency detection method. (*a*,*c*,*e*) DNS velocity signals, and (*b*,*d*,*f*) EXP1 velocity signals, processed in the same way. The signals correspond to $x = 500$ mm at the wall location of the u_{rms} peak.

(4) constructing an indicator function $\mathcal{I}(t)$ whose temporal mean is the intermittency γ. In this work, the above-mentioned steps are implemented to calculate γ from velocity–time signals as per the recent, relatively robust method proposed in the experimental study of Mamidala *et al.* (2022), wherein the Hilbert transform and adaptive threshold algorithm are utilized on velocity–time signals corresponding to the wall-normal distance where the u_{rms} peak value appears inside the BL for each streamwise location. This is, in our opinion, an improved version of the method applied in Fransson *et al.* (2005) and Fransson & Shahinfar (2020).

The detector function $\mathcal{D}(t)$ is merely a high-pass filtered velocity–time signal. The cut-off frequency f_{cut} for the high-pass filter has a constraint based on the local viscous length scale $\delta = \sqrt{xv/U_\infty}$, written as $f_{cut} = n \times U_\infty/\delta$, where n is a constant. The criterion function $\mathcal{C}(t)$ is based on the convolution of the Hilbert transform of $\mathcal{D}(t)$ over successive smoothing intervals. To calculate intermittency, one needs to construct an indicator function $\mathcal{I}(t)$ with a threshold $\mathcal{C}^{th}$ applied on $\mathcal{C}(t)$ as

$$\mathcal{I}(t) = \begin{cases} 1, & \text{if } \mathcal{C}(t) \geq \mathcal{C}^{th}, \\ 0, & \text{if } \mathcal{C}(t) < \mathcal{C}^{th}. \end{cases} \tag{2.1}$$

As an illustration, the turbulent event detection algorithms used for DNS and EXP1 signals are depicted in figures 2(*a*,*c*,*e*) and 2(*b*,*d*,*f*), respectively. The velocity signals correspond to the wall-normal peak location of the u_{rms}-profile at $x = 500$ mm. Note that the parameter n for the cut-off frequency used in $\mathcal{D}(t)$ is 0.04, and the threshold value is $\mathcal{C}^{th} = 0.15$ for both the DNS and experiments signals. These values are based on visual inspection of the velocity–time signals and then kept constant throughout all analysed cases in the present work. The calculated intermittency values are very close to each other with $\gamma = 0.21$ and 0.22 for the DNS and the EXP1 cases, respectively, despite the DNS signal being less than 0.4 s long while all experiments signals are 30 s long.

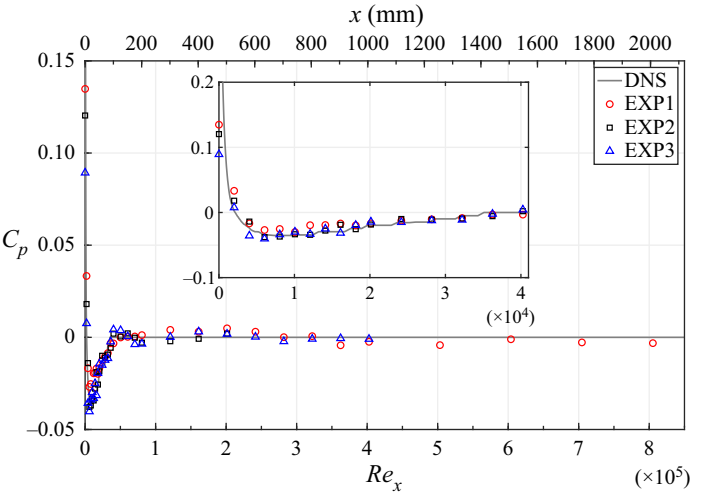

Figure 3. Comparison of C_p distributions in DNS with experiments. The inset corresponds to the LE region.

3. Experimental matching of DNS conditions

3.1. *Matching no. 1: pressure gradient*

The pressure gradient was adjusted to a close-to-zero pressure gradient flow along the streamwise extent of the plate utilizing the movable ceiling of the wind tunnel. Since the LE is a critical zone of the BL receptivity to free-stream turbulence, which recently has shown high sensitivity to the LE pressure gradient variations (cf. Mamidala *et al.* 2022), care was taken to fine-tune the location of the stagnation line on the LE. To match the pressure coefficient (C_p) distribution from the DNS, in this set-up, the trailing edge flap angle was tuned to 17.5°. In both DNS and experiments, C_p is calculated based on an inviscid and incompressible flow assumption using the mean velocity at the wall-normal location of $y/\delta_{99} = 3$ (i.e. following a streamline) as

$$C_p = 1 - \left(\frac{U(x)}{U_\infty}\right)^2. \tag{3.1}$$

Here, δ_{99} corresponds to the 99 % BL thickness. Note that at $x = 0$, a constant wall-normal height is used (next downstream location) since δ_{99} is zero at the LE. In figure 3, the C_p distribution for the DNS case is compared with experiments. The overall agreement is good. It can be inferred that the integral length scale has a negligible influence on mean C_p (which is consistent with Mamidala *et al.* 2022). The suction peak in the DNS is minimal ($C_{p,min} \approx -0.04$) when compared to the DNS of Ovchinnikov, Choudhari & Piomelli (2008), for instance, where the C_p distribution shows a relatively strong suction peak ($C_{p,min} \approx -0.4$). Note that a strong suction peak leads to a region of adverse pressure gradient, which is known to destabilize the BL, eventually causing increased disturbance growth rates in transition studies.

An account of the sensitivity of the LE pressure distribution to the LE receptivity process, for the present experiments, is given in Mamidala (2022) (cf. p. 145), which elucidates the importance of matching the full LE pressure distribution. The main conclusion is that all experiments cases (EXP1–EXP3), with the same *Tu* but different Λ_x, show high sensitivity to LE pressure gradient variations on the transition location.

3.2. *Matching no. 2: FST condition*

Free-stream turbulence is best assessed by its energy spectrum, but the characteristic FST parameters are often used to describe the FST conditions conveniently. In FST induced transition, the FST Reynolds number Re_{fst}, the turbulence intensity Tu and the streamwise integral length scale Λ_x expressed as a Reynolds number according to $Re_\Lambda = U_\infty \Lambda_x/\nu$ at the LE have been identified as the most important parameters (see e.g. Fransson & Shahinfar 2020). These parameters are related to each other as $Re_{fst} = Tu \times Re_\Lambda$. In the experimental case EXP1, not only the FST parameters Tu and Λ_x at the LE are replicated to match the DNS, but the entire energy spectrum at the LE (see § 2.3). For isotropic turbulence, the free-stream turbulence intensity can be written as

$$Tu = \frac{\sqrt{\overline{u^2}}}{U_\infty} = \frac{u_{rms}}{U_\infty}, \tag{3.2}$$

where u_{rms} is the root-mean-square value of the streamwise velocity component. Equation (3.2) is adopted as a relevant estimate for comparing DNS and experiments, since here a single hot-wire probe is used to obtain the streamwise velocities. In figure 4(*a*), the decay of turbulence intensity in the streamwise direction is compared for DNS and EXP1. Note that in experiments, the data are measured on the spanwise centreline $z = 0$ at $y = 100$ mm, which is enough for statistical convergence, while in the DNS, the turbulence decay shown is spanwise-averaged.

From the hot-wire velocity signals, the longitudinal integral length scale in the free stream is calculated using Taylor's hypothesis as

$$\Lambda_x = U_\infty \int_0^{\tau^*} R_{uu}(\tau)\, \mathrm{d}\tau, \tag{3.3}$$

where the truncated lag value τ^* corresponds to the first crossing of the abscissa of the autocorrelation R_{uu} of the velocity signal.

Close to homogeneous isotropic turbulence, the longitudinal integral length scale of turbulence Λ_x is expected to grow in proportion with $x^{1/2}$ (see e.g. Kurian & Fransson 2009, and references therein). This is observed for all experiments cases, but the DNS case shows a peculiar behaviour with initially a slower growth from the LE and then a larger growth from around $Re_x = 2.5 \times 10^5$ (see figure 4*b*). This can possibly be due to the fact that the turbulence used in DNS is synthetic. It should be pointed out that the Λ_x evolution is mostly not addressed in past DNS studies (Jacobs & Durbin 2001; Brandt *et al.* 2004; Ovchinnikov *et al.* 2008) or even overlooked (cf. figure 8*b* in Brinkerhoff & Yaras 2015). However, in a recent investigation by Durovic (2022), the sampling time issue was addressed, and it was pinpointed that it is important to check the generated synthetic FST, to see whether it is realistic enough without any spurious artefacts.

It is noteworthy that for EXP1, the transverse length scale obtained from the spanwise correlation in the free stream at the LE becomes $\Lambda_z = 2.67$ mm, which is close to half of Λ_x, which agrees with theoretical isotropic turbulence results.

Conventionally, the free-stream dissipation length scale L_ϵ can be defined as

$$L_\epsilon = \frac{k^{3/2}}{-U_\infty(\mathrm{d}k/\mathrm{d}x)}, \tag{3.4}$$

where k is the turbulent kinetic energy. In figure 4(*c*), the evolution of the length scale ratio in the free stream to the BL, i.e. L_ϵ/δ_1, is shown (δ_1 is the local BL

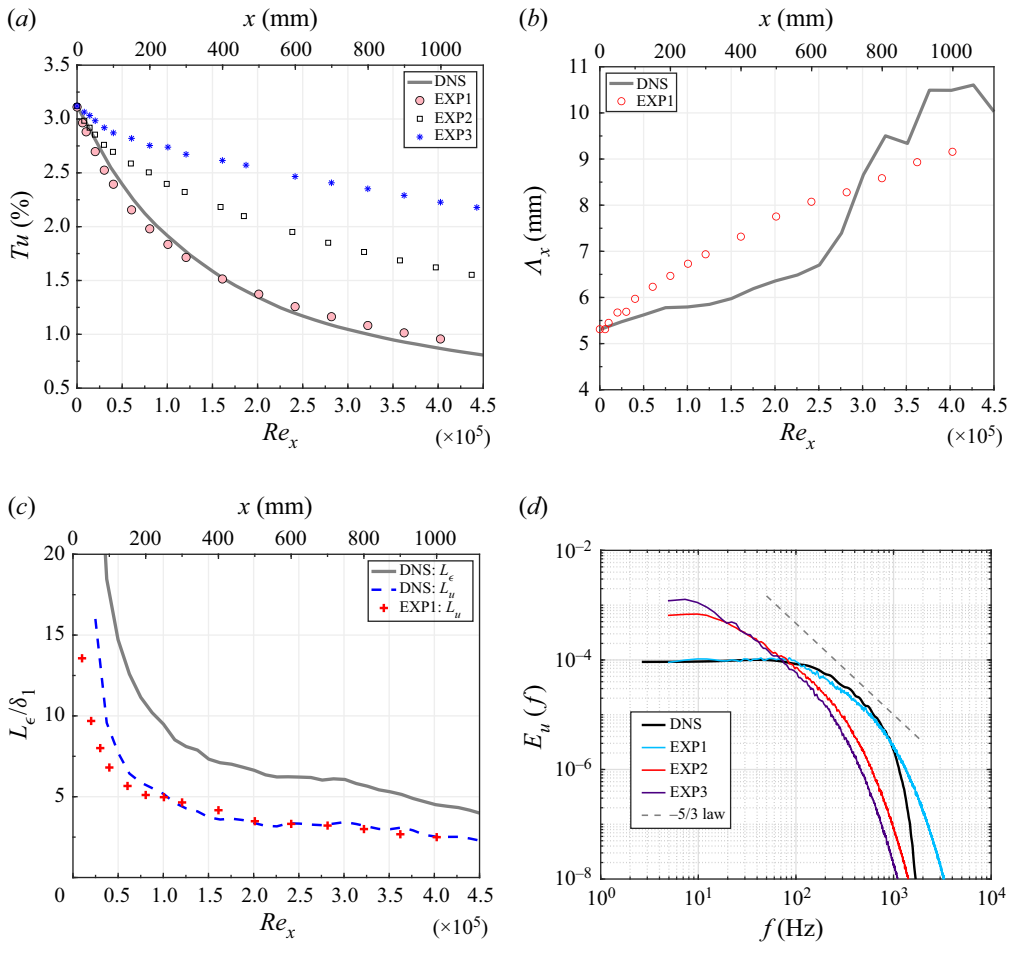

Figure 4. FST characterisation at the LE. (*a*) Decay of Tu with downstream distance. (*b*) Downstream growth of Λ_x. (*c*) Evolution of FST dissipation length scale normalized by local BL displacement thickness. (*d*) One-dimensional energy spectra of streamwise velocity signals compared at $x = 62$ mm (first available position in DNS).

displacement thickness). Note that in experiments, only the streamwise measure L_u is used for comparison. In the DNS, the ratio L_ϵ/L_u is approximately a constant value 0.54 throughout the length of the plate, which is less than the theoretical value for isotropic turbulence $\sqrt{2/3} \approx 0.82$, suggesting that the free stream is not isotropic (see § 4.3.1 in Jacobs 2000).

As addressed earlier, it is important to have homogeneity in both the spanwise and wall-normal directions of the FST, particularly if the inhomogeneity is periodic; the length scale may shadow the natural receptivity process by providing a preferential length scale. Figures 5(*a*,*b*), which show the Tu and Λ_x distributions in the vertical and spanwise directions, respectively, comply that the free-stream turbulence generated in the experiments is homogeneous. However, in DNS, it can be seen that the integral length scale fluctuates spuriously in the free stream (in both the y and z directions). The standard deviations for the mean for Tu and Λ_x in the wall-normal and spanwise directions are listed in table 2.

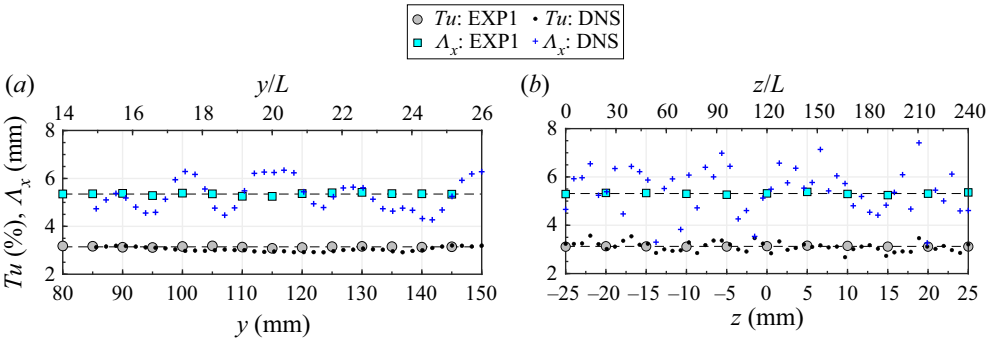

Figure 5. Incoming FST conditions at the LE ($x = 0$) in the free stream: (a) in the wall-normal direction (DNS $z/L = 120$, EXP1 $z = 0$ mm); (b) in the spanwise direction (DNS: $y/L = 25$, EXP1 $y = 100$ mm). Note that in DNS, the values are extrapolated at the LE.

Case	$Tu(y)$	$\Lambda_x(y)$	$Tu(z)$	$\Lambda_x(z)$
DNS	0.08 %	1.05 mm	0.14 %	1.25 mm
DNS[a]	0.05 %	0.60 mm	0.09 %	1.19 mm
EXP1	0.03 %	0.07 mm	0.02 %	0.06 mm

Table 2. Mean standard deviation values for FST conditions at the LE in the wall-normal and spanwise directions.

[a]Corresponding deviations at $x_s = 30.2$, i.e. at the downstream location where the first DNS time signals are available (i.e. no extrapolation to the LE is involved).

Finally, another fundamental comparison is the full free-stream energy spectrum. Since in the DNS the data are stored only on the plate, the streamwise location $x = 62$ mm has been chosen for the comparison. The one-dimensional energy spectra obtained from streamwise velocity signals are plotted in logarithmic scale in figure 4(d). There is a fair agreement between the DNS and EXP1 spectra, and it is noteworthy that the absolute values of $E_u(f)$ are close at low frequencies but start deviating from $f = 10^3$ Hz where the energy content is relatively low. From figure 4(d), as $f \to 0$, it becomes clear that the values of $E_u(f)$ are higher for EXP2 and EXP3 cases and lower for $f \gtrsim 10^2$ Hz, but with a more developed $-5/3$ region. For truly homogeneous and isotropic turbulence, the longitudinal length scale Λ_x can also be obtained from its energy spectrum as

$$\Lambda_x = \left[\frac{E_u(f)\, U_\infty}{4u_{rms}^2}\right]_{f\to 0} \tag{3.5}$$

(see e.g. Hinze 1987, p. 65). From the experimental spectrum of EXP1 at the streamwise location $x = 62$ mm, Λ_x is deduced as 5.5 mm (using (3.5)), which fits reasonably well onto the length scale evolution shown in figure 4(b).

4. Direct comparisons between experiments and DNS

4.1. *Comparison no. 1: BL parameters and skin-friction evolution*

Figure 6(a) depicts the streamwise development of the BL displacement and momentum thicknesses δ_1 and δ_2, respectively. The experimental data accord reasonably well in comparison to simulations for both displacement and momentum thicknesses up to about

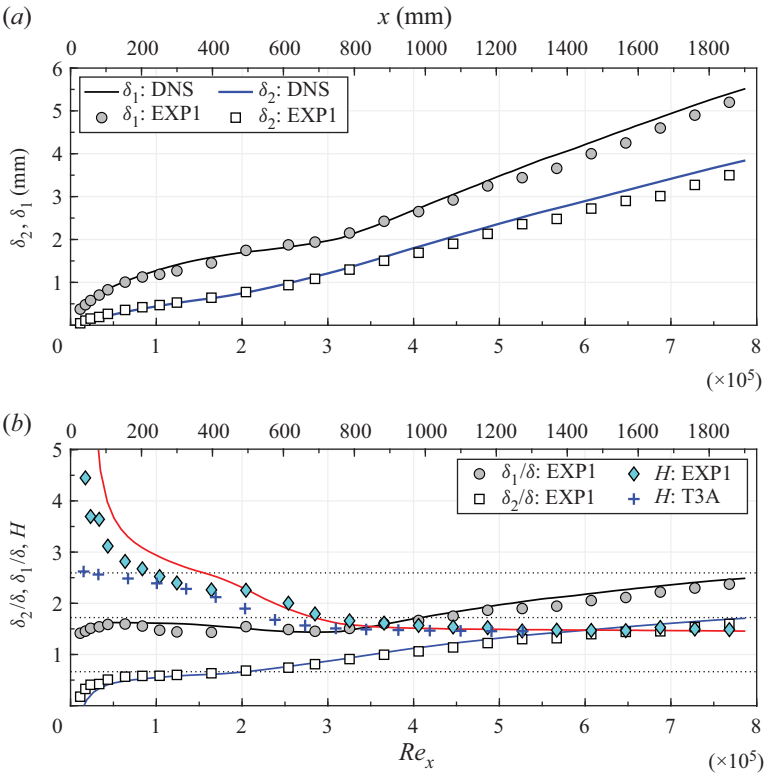

Figure 6. Comparison of BL parameters: (*a*) displacement thickness δ_1 and momentum thickness δ_2; (*b*) non-dimensional quantities δ_1/δ, δ_2/δ and shape factor H. Solid lines correspond to DNS. For the shape factor, T3A represents the data of Roach & Brierley (1992). The dotted lines show the Blasius values $\delta_1/\delta = 1.721$, $\delta_2/\delta = 0.664$ and $H = 2.59$.

$Re_x \sim 4 \times 10^5$. However, for $Re_x > 4 \times 10^5$ the growths of these BL parameters are clearly less in EXP1 compared to DNS. A possible explanation can be found going back to the external pressure gradient, which shows a slight favourable pressure gradient in the region $2 \times 10^5 < Re_x < 5 \times 10^5$, which would diminish the growth of the BL with some downstream delay. The reason is that the pressure gradient was tuned without any turbulence generating grid in the tunnel. With the grid, the BL transitions at $Re_{tr} = 2.5 \times 10^4$ and starts growing faster than without the grid, which is not compensated for by adjusting the ceiling of the test section further. In figure 6(*b*), the evolutions of non-dimensional parameters δ_1/δ, δ_2/δ and BL shape factor H are shown. Note that δ is the local BL scale corresponding to $\sqrt{x\nu/U_\infty}$. It is clear from figure 6(*b*) that a Blasius BL, indicated with dashed lines for the different parameters, is never obtained in a BL subject to FST, at least not for this high Tu level, despite a fairly close to zero pressure gradient flow (DNS perfectly zero downstream of $Re_x \approx 4 \times 10^4$). It can be observed that the values of H close to the LE are higher than the Blasius value 2.59 simply due to the inherent LE pressure gradient imposing inflectional velocity profiles in both experiments and simulations. In the case of turbulent BL flow, the shape factor lies in the vicinity of the value 1.49 but is expected to reduce as a fully turbulent BL eventually is established at higher Re_x. Note that H of EXP1 and DNS compares well downstream of $Re_x \sim 2 \times 10^5$; the difference can possibly be attributed to minor differences in mean C_p distributions in

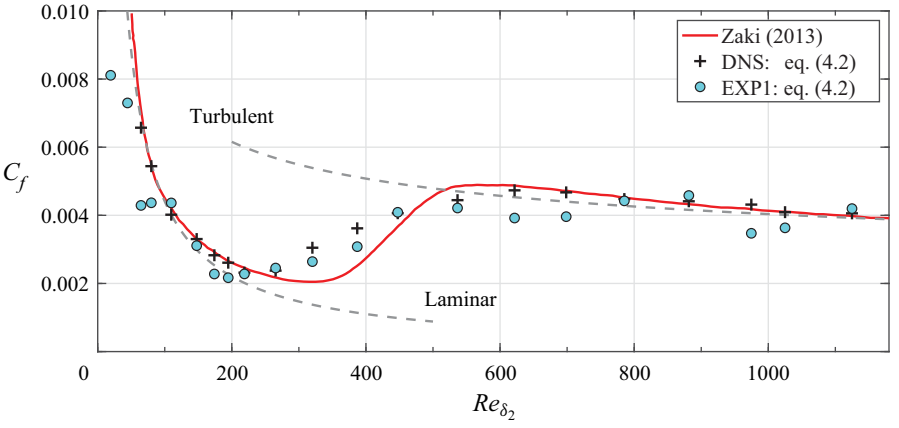

Figure 7. Skin-friction coefficient C_f versus the momentum thickness Reynolds number Re_{δ_2}. The dashed curves indicate the laminar and turbulent C_f relations in the text.

the LE region (see figure 3) and/or differences in Λ_x evolution. For additional comparison, the H values from the T3A experiment of Roach & Brierley (1992) are also plotted in figure 6(*b*).

A critical remark on the DNS data is that all mean velocity profiles from the LE show an overshoot, meaning that the free-stream velocity value far away from the wall is smaller than what is encountered at the BL edge. This overshoot gradually diminishes with the downstream distance; at $x = 62$ mm, the overshoot is 1.2 % of the free-stream velocity, and it is reduced to below 0.5 % downstream of $x = 580$ mm. All BL parameters in the DNS were calculated using the entire profiles, with the free-stream velocity calculated by averaging the last 20 points in the free stream.

It is well-known that the downstream evolution of the skin-friction coefficient C_f as plotted in figure 7 versus the momentum thickness Reynolds number Re_{δ_2} in linear scale imparts a clearer sense of the onset and extent of BL transition than the BL parameters. The established laminar and turbulent solutions for C_f are highlighted as dashed lines. The laminar part is the Blasius solution $C_f = 0.664^2/Re_{\delta_2}$, and the turbulent part is the logarithmic skin-friction law based on experimental investigation of Österlund *et al.* (1999), given as $C_f = 2 \times [(1/0.38) \times \log(Re_{\delta_2}) + 4.08]^{-2}$. In the present experiments, C_f was not measured independent of the velocity measurements; instead, the C_f evolution is estimated from the momentum-integral equation for an incompressible flow

$$\frac{C_f}{2} = \frac{\mathrm{d}\delta_2}{\mathrm{d}x} + \frac{\delta_2}{u_e}(H+2)\frac{\mathrm{d}u_e}{\mathrm{d}x}, \tag{4.1}$$

where u_e is the BL edge velocity. For the DNS data, the second term is less than approximately ± 2.5 % of the first term throughout the x range, which motivates the C_f to be estimated as

$$\frac{C_f}{2} = \frac{\mathrm{d}\delta_2}{\mathrm{d}x}. \tag{4.2}$$

This is a feasible approach in experiments when the friction velocity is not measured directly. Here, a central difference scheme has been used on the central points in figure 6(*a*), and a forward/backward scheme on the edges to calculate C_f in figure 7. Since the experiments give δ_2 only at discrete x locations, one will never capture the abrupt C_f

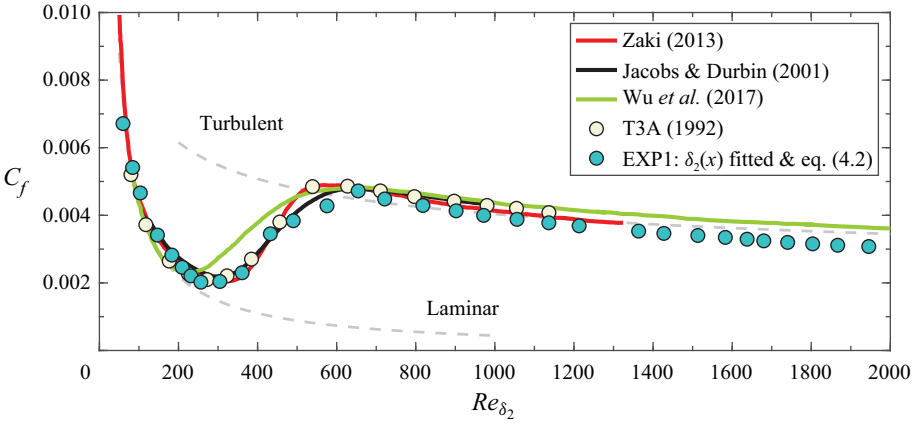

Figure 8. Skin-friction coefficient C_f versus the momentum thickness Reynolds number Re_{δ_2}. The dashed curves indicate the laminar and turbulent C_f relations in the text.

increase at transition. For a fairer comparison, C_f has been calculated using (4.2) with the DNS data using the same x locations as in EXP1. The solid line DNS result comes directly from the friction velocity. For larger Re_{δ_2}, the experimental data become quite scattered, which can be expected by looking carefully at the δ_2 data points in figure 6(a) (cf. $x > 1300$ mm).

One way to get close to full agreement with the solid line DNS result is by choosing appropriate functions of $\delta_2(x)$ and then curve fitting them to the data. Once the fitted functions look representative for the data, one can calculate $\mathrm{d}\delta_2/\mathrm{d}x$ analytically. In figure 8, the result of such a procedure is shown where three functions have been used with overlap, one for the laminar part, one for the transitional part, and one for the turbulent part. Here, the experimental data are compared with the previous works of Roach & Brierley (1992), Jacobs & Durbin (2001) and Wu *et al.* (2017). For the compared C_f data of the T3A case (Roach & Brierley 1992), obtained from Preston-tube measurements, the turbulence intensity at the LE can be extrapolated from the given Tu decay to 3.14 % (see also table 1 in Steelant & Dick 2001), which is close to the current EXP1 case, however for an unknown Λ_x. Furthermore, it should be emphasized that the simulations of Jacobs & Durbin (2001) and Wu *et al.* (2017) did not include a LE, but the inlet FST intensities are similar to Roach & Brierley (1992). It can be seen that the C_f from the DNS case (Zaki 2013) and the EXP1 case develop similarly except in the turbulent region where the C_f values are slightly lower for EXP1. This can again be attributed to the slight favourable pressure gradient downstream of $Re_x = 2 \times 10^4$, which diminishes the growth of the momentum thickness leading to a somewhat smaller $\mathrm{d}\delta_2/\mathrm{d}x$. The laminar region and the transition onset for the EXP1 case certainly appear to be consistent with Roach & Brierley (1992), Jacobs & Durbin (2001) and Zaki (2013). However, the data of Wu *et al.* (2017) clearly have an earlier onset which, according to the authors, could be due to the fact that they matched the FST intensity only with T3A experiments and not the length scale, which on the other hand is unknown in the T3A case since it was never measured. There is, however, a hand-waving estimation of the integral length scale for the T3A case based on an estimation of the dissipation length scale (Savill 1993; Johnson & Ercan 1999), which circulates but which is not repeated here since it does not come from the original source (Roach & Brierley 1992). Considering the earlier onset of transition of the Wu *et al.* (2017) data, despite the slightly lower Tu level, it is expected that their Λ_x is significantly longer than in EXP1

Case	U_∞ (m s^{-1})	Tu (%)	Λ_x (mm)	Re_{fst}	LE
Zaki (2013)	6.2[a]	3.12	5.32[a]	67[a]	Yes
EXP1	6.2	3.13	5.31	67	Yes
T3A	5.2[b]	3.14[c]	—	—	Yes
Jacobs & Durbin (2001)	—	3.5	—	—	No
Wu *et al.* (2017)	—	3.0	—	—	No

Table 3. FST conditions for the compared cases in figures 7 and 8. In the simulations without LE, the conditions at the inlet of the simulation domain are taken.
[a]The U_∞ is chosen in the present comparison, and Λ_x is calculated as outlined in § 2.3.
[b]This value is the averaged free-stream velocity along the plate.
[c]The extrapolated Tu level at the LE from the full Tu decay function.

and the DNS by Zaki (2013) since for this relatively short Λ_x, the $\mathrm{d}Re_{tr}/\mathrm{d}(\Lambda_x/\delta_{tr})$ is expected to be negative, which would move the transition location upstream (cf. Fransson & Shahinfar 2020). Known numerical values of the FST conditions for the different cases in figure 8 are given in table 3.

4.2. *Comparison no. 2: intermittency factor evolution*

Figure 9 shows the streamwise intermittency distributions for all cases. The procedure outlined in § 2.4 has been adopted in evaluating the cases. To obtain the transition location x_{tr} defined at $\gamma = 0.5$ for the experimental cases, a sigmoid function in the form $\gamma(x) = 1 - \exp[-\alpha\,(x-\beta)^c]$ is fitted to each individual γ distribution, where α, β, c are the curve fitted coefficients. This shape of the intermittency function is based on the theoretical work by Narasimha (1957), Dhawan & Narasimha (1957) and Johnson & Fashifar (1994), but where the exponent c comes out as 2 and 3, respectively. In several comparisons with these models (see e.g. Fransson *et al.* 2005; Fransson & Shahinfar 2020), it is, however, shown that one obtains a better fit to the data for a larger c value, which is why it is here part of the curve fitting procedure. The respective transition locations x_{tr} at $\gamma = 0.5$ are tabulated in table 1. As illustrated in figure 9, transition happens earlier for larger integral length scales, and the agreement between DNS and EXP1 is excellent despite minor differences in C_p distributions and the FST evolution (in particular for Λ_x). Worth recalling here is that the DNS γ distribution has been calculated using the same MATLAB® code as for the experimental cases following the method outlined in § 2.4. The largest deviation takes place at transition onset, i.e. for $\gamma < 0.1$, but the agreement has still to be judged as good. From $\gamma = 0.2$ the agreement is remarkable, and at transition (i.e. at $\gamma = 0.5$) the EXP1 and DNS give interpolated transition locations $x_{tr} = 624$ and 620 mm, respectively. For EXP2, EXP3, EXP4, the corresponding transition locations are 481, 465, 1792 mm, respectively. All values are summarized in table 1 along with their respective FST characteristic parameters. EXP4 is the case that seems to be an outlier here but will be addressed in depth in § 5.1.

4.3. *Comparison no. 3: wall-normal BL profiles*

In this subsection, wall-normal profiles up to fourth-order velocity moment measured in the laminar, transitional and turbulent regions are compared. Wall-normal velocity profiles of mean U and disturbance amplitude u_{rms} are shown in figures 10(a) and 10(b), respectively, for the EXP1 case and compared with DNS. For convenience, the velocities are normalized by the local free-stream speed U_∞. The mean velocity

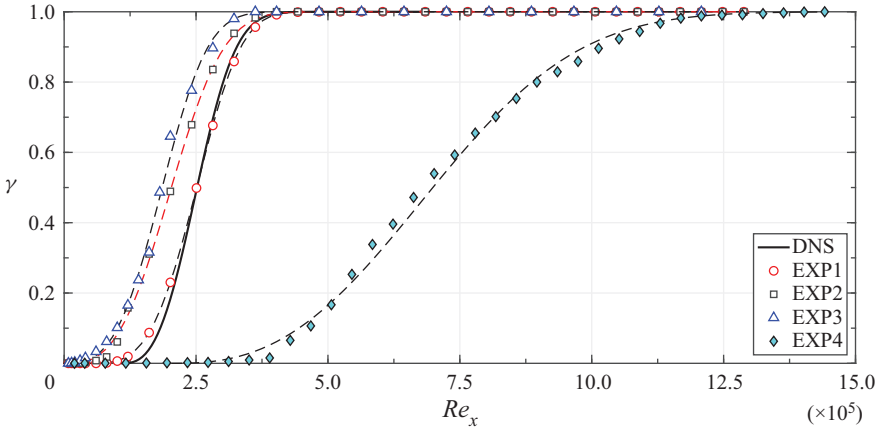

Figure 9. Direct comparison of γ distributions between DNS and EXP1 along with all other experimental cases. Dashed lines indicate a sigmoid fit to each individual γ distribution in the experiments.

profiles corresponding to the EXP1 case agree well with the DNS (solid lines) across the entire x range, except for the two first profiles at $x = 100$ and 200 mm where the two profiles deviate. The EXP1 profiles seem to have larger shape factors, which is consistent with figure 6(*b*). The shape factor comparison showed differences down to $Re_x \sim 2 \times 10^5$, which explains the mismatch of the most upstream mean velocity profiles.

In experiments, the peak values in the u_{rms} profiles in the transition to turbulent region are nominally lower than the DNS (see figure 10*b*), which cannot be attributed to a limited spatial resolution of the hot wire since the viscous length of the wire is $L_w^+ = 11$–15 for these low Re_x. The near-wall peak intensity in the r.m.s. profiles steadily increases and then diminishes as it approaches the turbulent state. Apart from this, the peak u_{rms} location moves closer to the wall with increasing Re_x. This behaviour is known and has been reported in a number of previous works but is anyway highlighted in a separate figure here since it includes the direct comparison between experiments and DNS; see figure 11. In this figure, all the experiment cases are added and show the location of the disturbance peak (figure 11*a*) and the peak value (figure 11*b*). It is noteworthy that in all the profiles shown in figures 10(*a*,*b*), some quantitative differences were observed between the DNS and EXP1 cases. If the data from the DNS are chosen at only a single spanwise coordinate, e.g. $z/L = 0$, then wall-normal undulations are noticeable, especially in the free stream and around the u_{rms} peak, which is removed after spanwise averaging. This suggests that the time span of the simulation is too short for local convergence, whereas in the experiments, this is not a problem.

Most transition studies attempt only to evaluate the spatial distributions of U and u_{rms}, i.e. the first and second moments of velocity, respectively. However, in this investigation, direct comparisons of higher-order moments, such as the third and fourth moments of velocity, namely the skewness $\mathcal{S}_u$ and kurtosis $\mathcal{K}_u$, have also been compared. For these direct comparisons, including a more thorough comparison of first- and second-order moments, the interested reader is referred to Mamidala (2022) pp. 140 and 141 (figures 13 and 14, respectively).

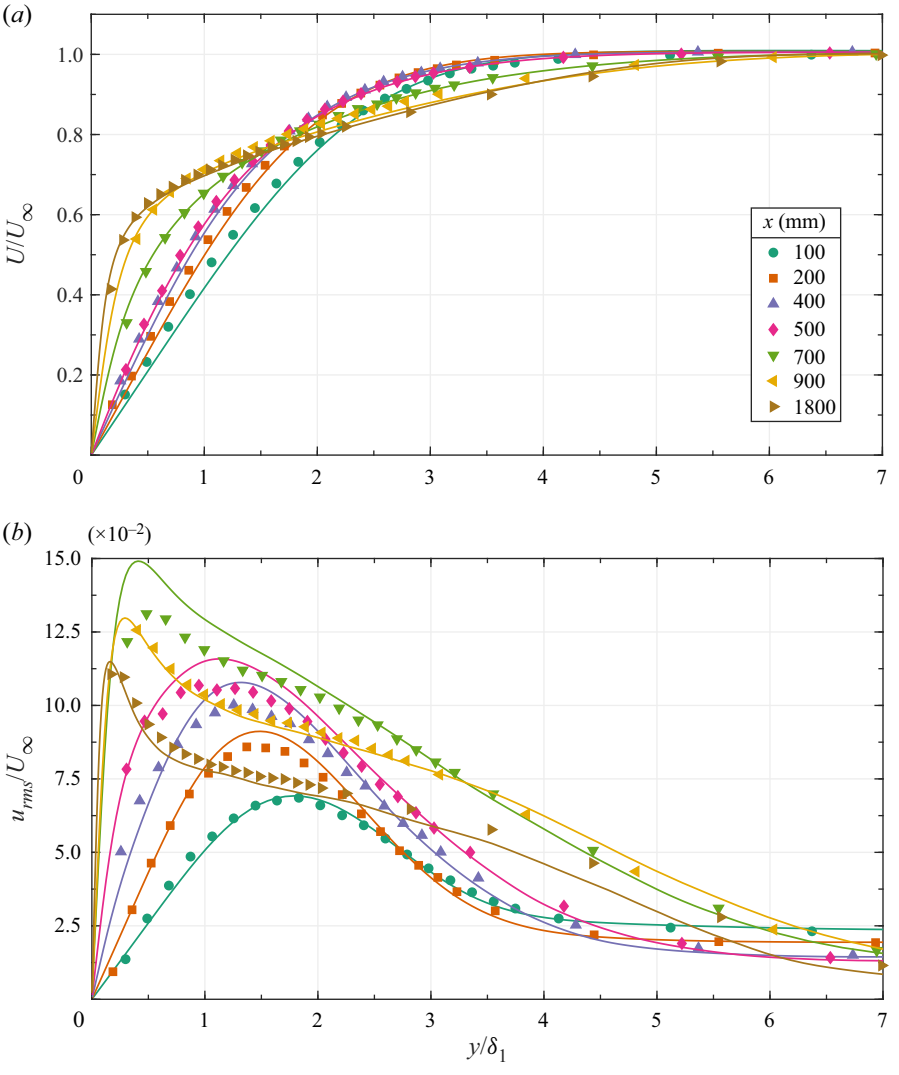

Figure 10. The downstream evolution of wall-normal profiles: (*a*) mean velocity U/U_∞, and (*b*) r.m.s. velocity u_{rms}/U_∞, through laminar to turbulent transition for the case EXP1 compared to DNS (solid lines). The abscissa is normalized with its local displacement thickness δ_1. Corresponding γ values can be found in figure 9.

4.4. *Comparison no. 4: BL streak spacing*

The two-point hot-wire correlation results in the experiments of Klebanoff (1971), Kendall (1985) and later Kosorygin & Polyakov (1990) reveal that the two-point correlation coefficients in span inside the BL show a clear minimum in an FST environment. This minimum Δz_{min}, determined at a wall-normal location of the u_{rms} maximum, is associated with the averaged spanwise separation between adjacent streamwise streaks. More precisely, Δz_{min} is the distance to the first maximum anticorrelation and can be interpreted as a measure of the half-spanwise wavelength of the streaks, i.e. $\lambda_z/2$.

In this study, the spanwise correlation $R_{uu}(z)$ from DNS and experiments is obtained using different methods. In DNS, first, at each single time step t_i, the spatial autocorrelation

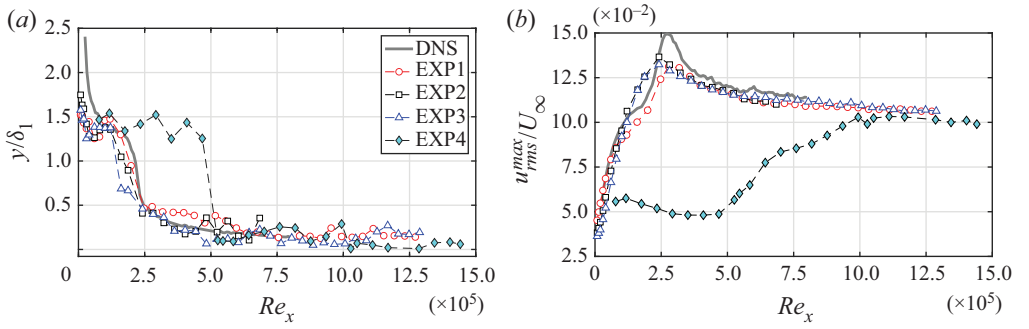

Figure 11. (*a*) The wall-normal location of the peak value in u_{rms}. (*b*) The downstream evolution of the peak value in u_{rms}.

$R_{uu}(z)$ is calculated at the y location of the corresponding u_{rms} peak. Then the time-averaged value of $R_{uu}(z)$ is used to evaluate the z location of $\min\{R_{uu}(z)\}$. This method is adopted to eliminate spurious undulations in $R_{uu}(z)$, which exist for certain time steps in DNS as $z \to \infty$. In experiments, two hot-wire probes are needed to measure this spanwise cross-correlation. Practically, the signals from two probes are measured simultaneously by placing one fixed probe and one movable probe along the span. This is a long-adopted procedure since the first experiments of Klebanoff (1971). In the laminar region, where the signals have no signs of intermittency, the two-point cross-correlation can be performed straightforwardly. But if the hot-wire signals contain any turbulent signatures, then they should be removed from the signals (similar to Yoshioka, Fransson & Alfredsson 2004). The conditional correlation function is obtained by extracting the laminar portions of the fixed probe, and only these periods are used to determine the cross-correlation. Otherwise, even though a clear minimum exists inside the BL, it is not evident since the high-frequency content of a turbulent spot can show a high correlation value.

Figure 12(*a*) shows the downstream development of $R_{uu}(z)$ measured inside the BL. The cross-correlation functions from the EXP1 (filled symbols) are compared with spanwise autocorrelations from DNS (solid lines) at the marked x locations in the plot. Before transition onset ($\gamma = 0.05$), which is equivalent to $x = 355$ mm, the minima in $R_{uu}(z)$ from the experiments are slightly smaller than the DNS values, while moving downstream, good agreement is observed. The dashed lines in figure 12(*a*) correspond to the free-stream correlation function. The downstream growth of streamwise streaks is shown in figure 12(*b*). As is evident, for the smallest integral length scale (DNS & EXP1), the streak spacing increases up to 35 %, whereas for the larger Λ_x case (EXP3), the streak growth is extenuated. Note that for the analysed cases in figures 12(*a*,*b*), Δz_{min} is evaluated only up to a moderate level $\gamma = 0.25$ %, i.e. up to where transition has been initiated.

4.5. *Comparison no. 5: integrated energy*

In this subsection, the early disturbance growth due to FST is addressed. Looking at the data by Brandt *et al.* (2004) (figure 4*a*), it is clear that the initial disturbance growth is larger for the smallest Λ_x, suggesting that the smallest scales penetrate the BL edge more easily. This result does not contradict the 'shear-sheltering' concept, though, since a particular FST energy spectrum has its scales with its characteristic integral length scale (Λ_x), which might not match the optimal scale for the fastest route to transition that nature

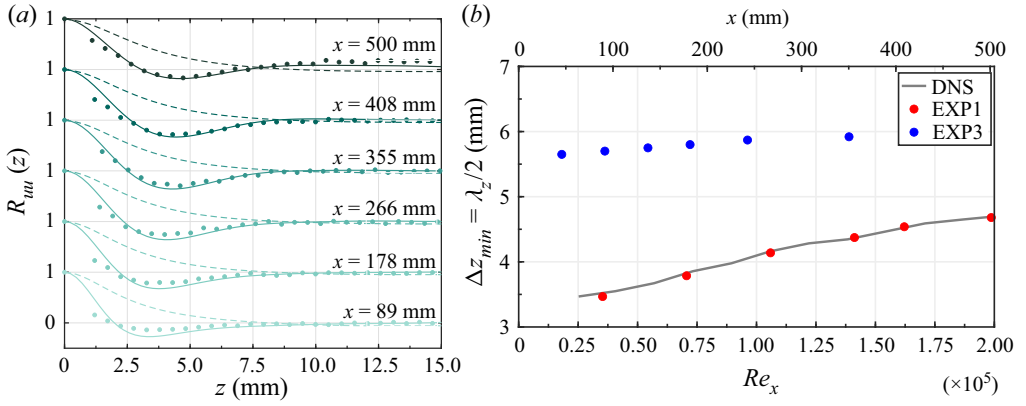

Figure 12. (*a*) Spanwise correlation functions of the streamwise velocity at various x locations. Filled ○ symbols indicate EXP1; solid lines indicate DNS; dashed lines indicate DNS in free stream. (*b*) Downstream evolution of half-spanwise wavelength of streaks versus Re_x.

is expected to take in its strive for disorder (increased entropy). Instead, it seems to be a matter of scale-matching since transition can move both upstream and downstream for increasing Λ_x depending on the energy spectrum (Fransson & Shahinfar 2020).

The role of the streaks and their spanwise wavelength (λ_z) in the FST transition scenario is believed to be important for the transition onset by the present authors. The ratio λ_z/Λ_x decreases with Re_{fst}, which indicates that Λ_x is important in setting λ_z of the streaks (see eq. (3.7) in Fransson & Shahinfar 2020; Mamidala 2022). This also proves that it is the large scale in the FST that has the most impact on the formation of the streaks, but the growth of the streak amplitude inside the BL will depend on the scale-matching, which seems to have its optimum around $(\Lambda_x/\delta_{tr})_{opt} = 12.5$ at transition onset (Mamidala *et al.* 2022), where δ_{tr} is the BL scale at transition. It is noteworthy that λ_z strongly correlates with Λ_x and that the optimal scale ratio can be interpreted as a BL structure aspect ratio in the cross-sectional plane.

In figure 13(*a*), the disturbance growth, in terms of the ratio of maximum fluctuation of the streamwise velocity u^{max}_{rms} to the fluctuation in the free stream at LE u^0_{rms}, is displayed for all the experimental cases and compared against the DNS. In the region $Re_x < 1 \times 10^5$ (highlighted in light green), the slopes of all growth curves are almost the same (almost linear and parallel), and for smaller integral length scales, the ratio u^{max}_{rms}/u^0_{rms} is larger in this region very similar to Brandt *et al.* (2004). It is noteworthy that the DNS and EXP1 data grow in the same manner; however, they branch out subsequently, with the EXP1 data showing a lower disturbance level. However, the DNS and EXP1 follow the same trend and have their disturbance maxima around the same Re_x. The result from figure 13(*a*) affirms the result of Brandt *et al.* (2004) through experimental validation, suggesting that small scales can penetrate the BL more easily in the early stage of disturbance growth. Brandt *et al.* (2004) argue that the free-stream turbulence decays faster for smaller integral length scales, and therefore it is less effective in continuously forcing the streaks along the plate. Their data show that the longer integral length scales overtake the smaller length scale in terms of disturbance growth further downstream, where the BL is thicker, which is also seen in the present experiments.

The streamwise evolution of the integrated energy E_{int} of the disturbances is presented in figure 13(*b*). Here, the integral parameter E_{int} is obtained by integrating the squared

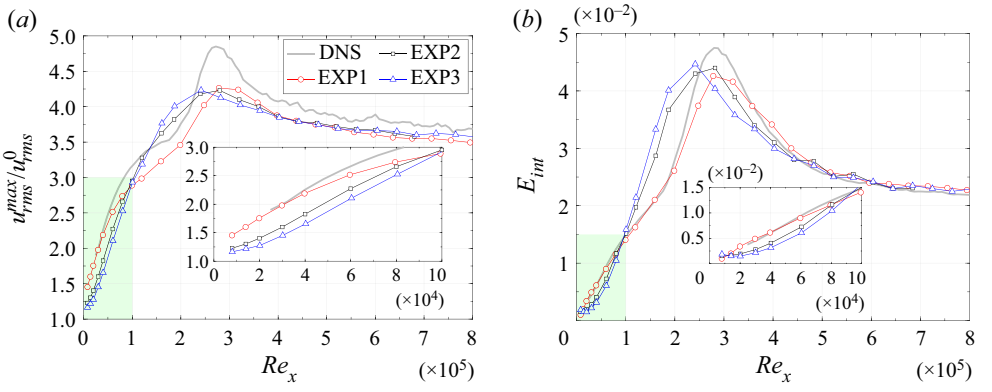

Figure 13. Disturbance growth versus Re_x, showing: (*a*) the u_{rms} peak evolution, and (*b*) the integrated energy. Note that in each plot, the highlighted region in light green is zoomed in and displayed in the inset.

u_{rms} profiles in the wall-normal direction as

$$E_{int} = (1/U_\infty^2) \int (u_{rms}^2 - u_{fst}^2)\, \mathrm{d}(y/\delta_1), \tag{4.3}$$

where u_{fst} is the disturbance amplitude in the free stream. Note that in this paper, the disturbance energy is not obtained from the commonly known definition of energy as u_{rms}^2/U_∞^2, since E_{int} brings out an integrated effect. It can be observed that EXP1 and DNS compare well with each other except for the lower maximum E_{int}-value in EXP1. Quite similar to the aforementioned ratio $u_{rms}^{max}/u_{rms}^{0}$, the energy content is larger closer to the LE (highlighted in light green) for a smaller FST length scale. For EXP1, the growth of this energy parameter is linear, while the longer Λ_x cases show a quadratic behaviour. This agrees with experiments of Fransson *et al.* (2005) and simulations of Ovchinnikov *et al.* (2008). Fransson *et al.* (2005) associate this with the receptivity process, which needs a certain downstream distance before completion and the disturbances adjust to the BL. Ovchinnikov *et al.* (2008) term it as 'receptivity distance', which is essential for length scale adjustment between the free stream and the BL. According to Zaki & Saha (2009), the integrated disturbance amplitude is related to the penetration of FST into the BL. Likewise, the integrated energy E_{int} can also be connected to the penetration of disturbances. It is clear from figure 13(*b*) that for small Λ_x, E_{int} is initially higher, indicating that the FST disturbances penetrate the BL more easily for small Λ_x, as concluded previously from the $u_{rms}^{max}/u_{rms}^{0}$ evolution.

4.6. *Comparison no. 6: pre-multiplied power spectral density*

In this subsection, the pre-multiplied Welch power spectral density (PSD) is compared at some selected downstream locations throughout the BL. In figure 14 the x locations are given in the plots, and the corresponding Reynolds number range is $Re_x = (80\text{–}620) \times 10^3$. Recall that the transition location is defined as where $\gamma = 0.5$ corresponds to $x \approx 620$ mm (or $Re_x \approx 260 \times 10^3$). The frequency is non-dimensionalized with the free-stream velocity and the local BL displacement thickness. As expected, the energy content increases in maximum intensity and broadens out in the wall-normal direction. The location of the peak value in terms of both y/δ_1 and $\mathcal{F}$ is highlighted in figures 15(*a*) and 15(*b*), respectively. The agreement with the DNS data has to be considered very good.

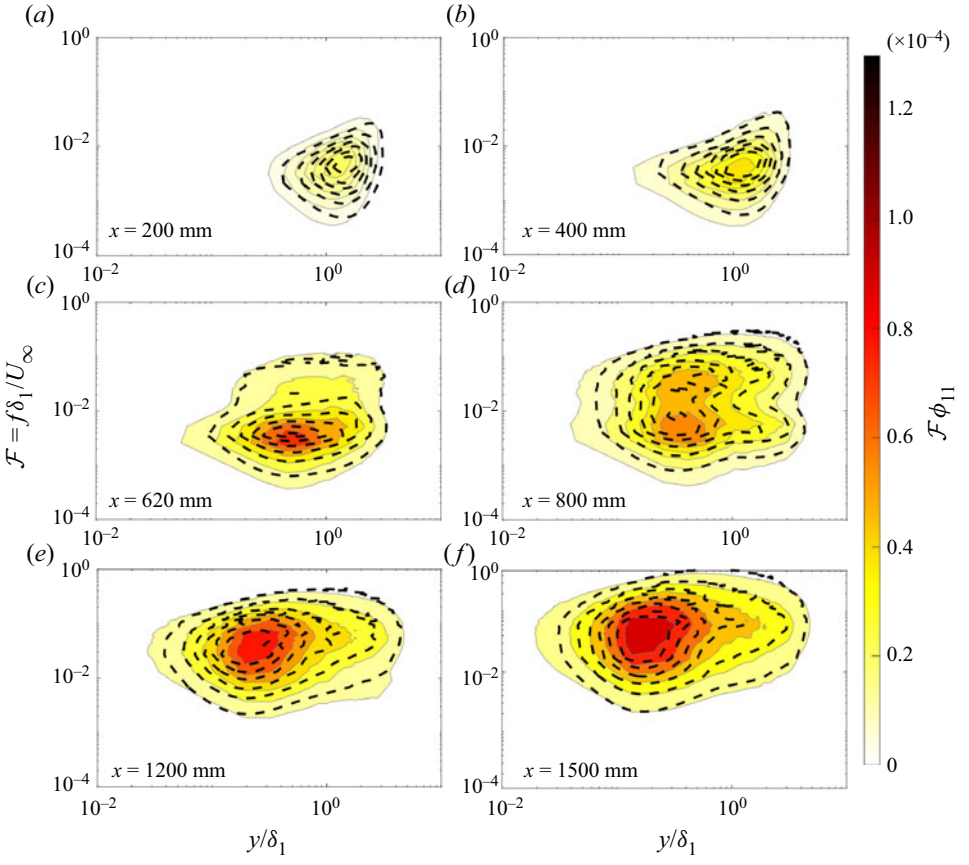

Figure 14. Comparison of contour maps of the pre-multiplied wall-normal power spectra $\mathcal{F}\phi_{11}$ in DNS and EXP1. The filled contour plots correspond to EXP1, and the dashed contour lines correspond to DNS.

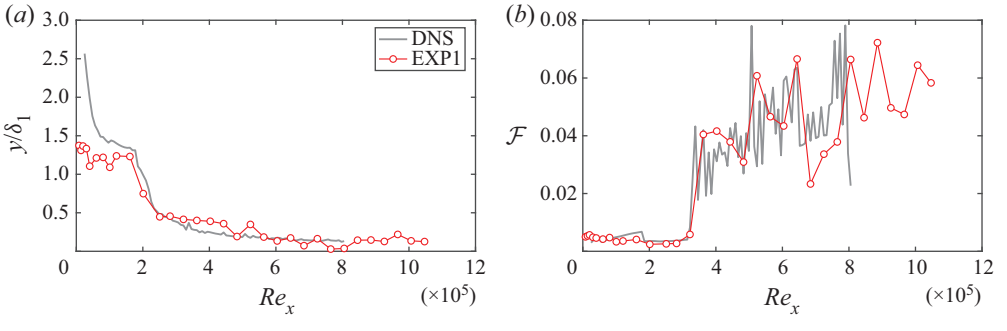

Figure 15. (*a*) The wall-normal location of the peak value of $\mathcal{F}\phi_{11}$. (*b*) The downstream evolution of the peak value of $\mathcal{F}\phi_{11}$.

The type of contour plots shown in figure 14 is frequently plotted for canonical turbulent BLs and compared with other works. In transition studies, it is not common (the present authors are not aware of any), but it does not really make sense unless the transition location matches as it does in this comparative study.

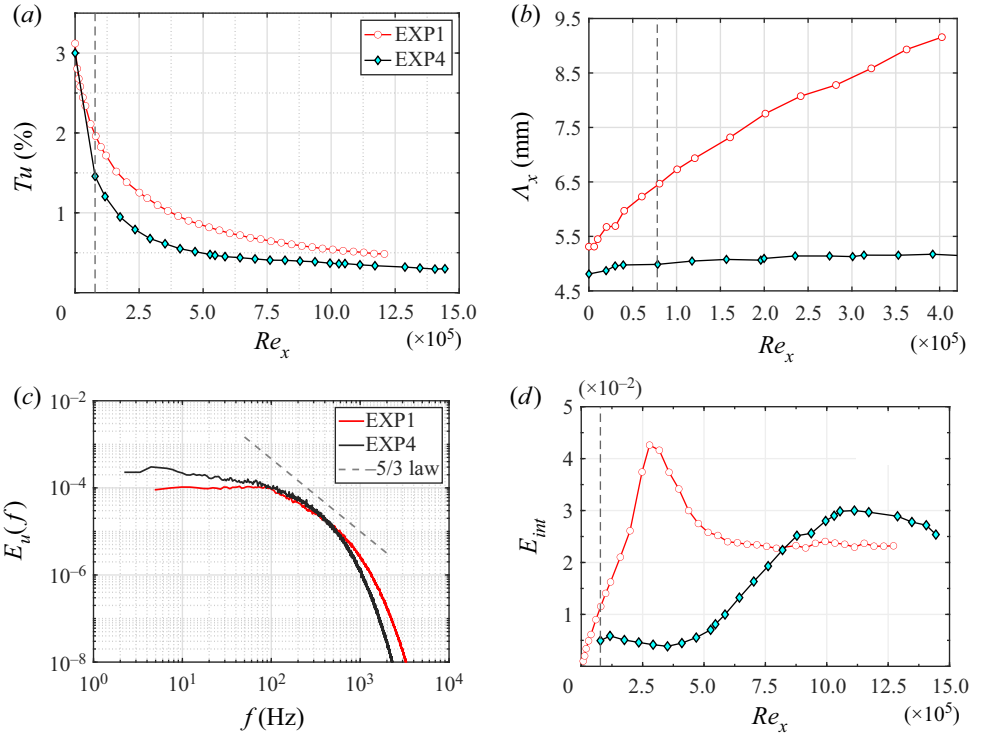

Figure 16. Direct comparison between EXP1 and EXP4: (*a*) *Tu*-decay; (*b*) Λ_x-increment; (*c*) full energy spectra; (*d*) E_{int}-evolution. Note the different Re_x range in (*b*). Dashed lines correspond to $Re_x = 0.8 \times 10^5$.

5. Boundary layer receptivity

5.1. *Importance of full FST energy spectrum (experiments)*

Here, we want to elucidate the importance of matching the full FST energy spectrum at the LE if the aim is to perform a direct comparison between two cases, be it between DNS and experiments or between two experiments or two DNS. Only matching the turbulence intensity and the FST integral length scale can give very different *Tu* decays and Λ_x increments, which will affect the continuous downstream FST forcing on the BL edge very differently, but maybe more importantly, the LE receptivity, which probably depends on the entire FST spectrum rather than representative integral parameters. In figure 16, the two cases EXP1 and EXP4 are compared with each other, with seemingly similar FST conditions at the LE if one looks only at the *Tu* level (≈3 %) and Λ_x (≈5.0 mm). However, since the energy spectra are very different, even crossing each other, as shown in figure 16(*c*), there is a mismatch in the downstream evolution of *Tu* and Λ_x (see figures 16(*a*) and 16(*b*), respectively) which causes completely different BL disturbance evolution (cf. figure 16*d*). Noteworthy is the peculiar case EXP4, which shows an initial disturbance energy growth followed by a decay until it decides to grow and transition to turbulence. Comparing the initial decay of *Tu* (figure 16*a*), one can see that the EXP4 case has dropped by 100 % already at $Re_x = 0.8 \times 10^5$, while the corresponding drop for EXP1 is approximately 35 %, and that at $Re_x = 4 \times 10^5$, the *Tu* level is approximately 50 % larger in EXP1 compared to EXP4. The LE values of Λ_x differ with only approximately 10 % between the two cases, but the difference in the downstream growth is immense, leading

to a difference of 75 % at $Re_x = 4 \times 10^5$. As a result, the transitional Reynolds number is 175 % larger for EXP4 compared to EXP1.

In the work by Fransson & Shahinfar (2020), it was proposed that it would be enough to know the LE FST condition in terms of Tu and Λ_x in order to be able to predict the transition location. In figure 3 of Fransson & Shahinfar (2020), it is clear that the Tu and Λ_x downstream evolutions, for their different turbulence generating grids, have pretty similar behaviour, i.e. the curves from different grids are merely shifted with the LE Tu value. This is likely to be the reason why that proposed transition prediction method was shown to work so well. Figure 16(d) illustrates the importance of the LE energy spectrum, and shows that LE Tu and Λ_x values are not enough to characterize the FST condition for transition prediction unless the Tu decay does not severely differ more than with its absolute value.

5.2. *FST BL penetration (DNS)*

There are quite a few studies reporting correlation data throughout BLs subject to FST. From the experiments of Charnay, Mathieu & Comte-Bellot (1976), Hancock & Bradshaw (1989), Thole & Bogard (1996) and Sharp, Neuscamman & Warhaft (2009), the uv autocorrelation coefficient R_{uv} has a strong negative minimum approximately -0.45 inside the BL for low Tu levels, which becomes less negative for higher Tu levels. The strong negative minimum is due to the general nature of the wall-normal velocity component of the free-stream fluid entering the BL, which induces a positive increment on the streamwise velocity component. However, if one wants to discuss penetration depth, then the two-point velocity correlation would be more appropriate since it correlates signals at different points of the flow field.

To elucidate more on the notion of penetration depth, as an example, the two-point velocity correlation maps of different correlation coefficients are compared from DNS data calculated with the reference velocity signal denoted by superscript $*$ at a fixed location outside the BL. The coefficients C_{u^*u}, C_{v^*v} and C_{v^*u} are plotted in figures 17(a), 17(b) and 17(c), respectively, with the location of the reference signal indicated by a cross-marker outlined by a circle. The data used to calculate the correlation coefficients in figure 17 correspond to the data in the xy-plane of window A in figure 18.

Consistent with Nolan & Walsh (2012) and Balamurugan & Mandal (2017), both C_{u^*u} and C_{v^*v} maps have their maxima at the location of the reference signal location since the time lag between the two signals is zero. However, one may observe that the C_{v^*u} map has a negative minimum inside the BL, which simply indicates that a vertical perturbation towards the wall at the reference location directly induces a positive velocity perturbation inside the BL. Hence next, the spatial development of C_{v^*u} is examined in both the streamwise and wall-normal directions. The interrogation windows investigated are shown in the contour plot of U/U_∞ in figure 18.

For simplicity, the focus will first be on the three windows denoted A, B and C in figure 18. In all the contour maps of C_{v^*u} displayed in figure 19, the dashed lines indicate the wall-normal locations of $y = \delta_{99}$. The wall-normal coordinates are normalized by corresponding BL thicknesses δ_{99}, and x coordinates are normalized by length scale L (from DNS). The v component of the velocity at the reference point (cross-marker outlined by a circle) is used to correlate the u component of all the other spatial points to obtain the correlation maps. The minimum of C_{v^*u} is highlighted as a filled white bullet. In addition, if only window A is considered, then the reference point is moving from $y/\delta_{99} = 1.8$ (top)

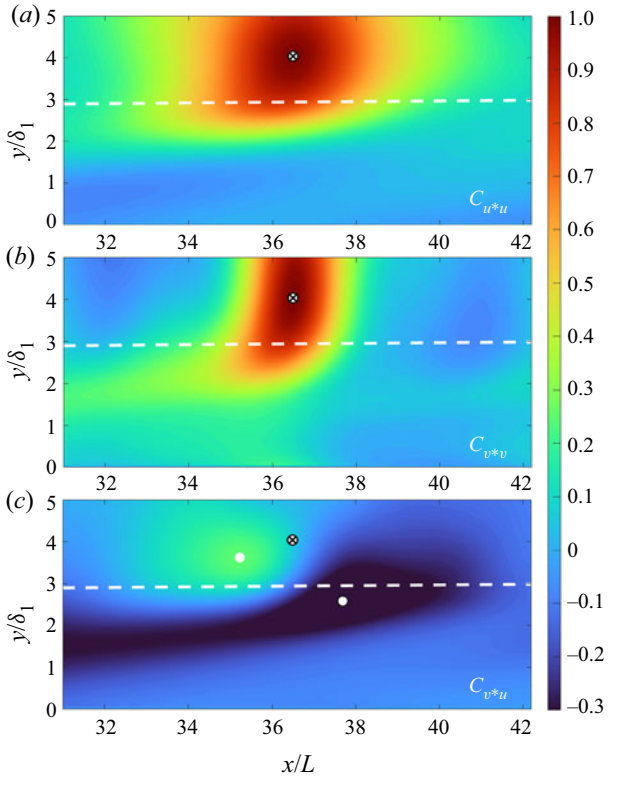

Figure 17. Two-point correlation maps from DNS: (*a*) C_{u^*u}, (*b*) C_{v^*v}, and (*c*) C_{v^*u}. The dashed white line corresponds to δ_{99}. A cross-marker outlined in a circle indicates the reference point, which is in the middle of the window at $y/\delta_1 = 4$ (here, $y/\delta_{99} \approx 1.5$). The white bullets represent the maximum value 0.28 and minimum value -0.43 of C_{v^*u}.

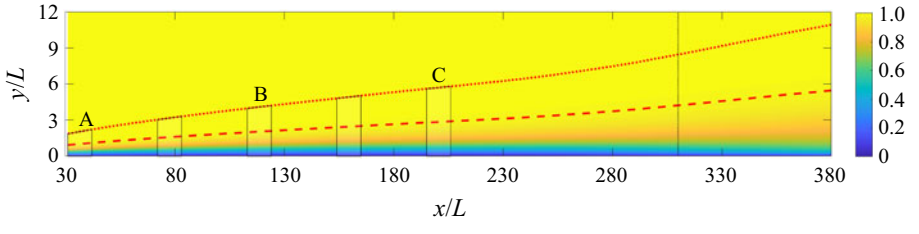

Figure 18. Contour plot of mean velocity U/U_∞ from DNS. Dashed and dotted lines correspond to δ_{99} and $2\delta_{99}$, respectively. Marked squares in black represent the interrogation windows considered.

to 1.5 (middle), to 1 (lower). Moving downstream, i.e. from window A to window C, the physical distances from the BL edge to the reference points taken from window A are maintained constant.

Looking at window A with the reference location moving closer to the wall (from top to bottom) in figure 19, the magnitude of the peak minimum is increasing, and its location gradually moves closer to the wall. One may also observe a small upstream shift of this peak minimum. Regarding the positive maxima, it is of less interest since it is always located outside the BL, but it is also expected since a vertical perturbation towards the wall will slow down the streamwise velocity component and cause a negative perturbation

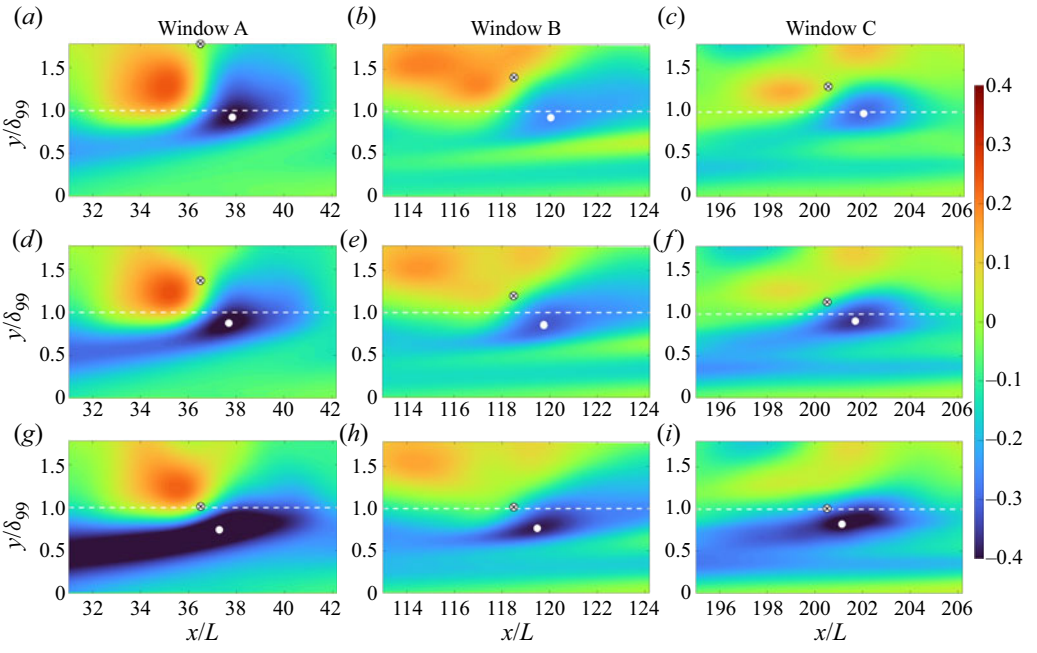

Figure 19. Two-point velocity correlation C_{v^*u} maps from DNS. The dashed white line in each plot corresponds to $y = \delta_{99}$; the cross-marker outlined by the circle represents the reference point; a white circle represents the minimum value of C_{v^*u}. In each case from windows A to C, the reference point (cross-marker) is kept at the same physical distance above the BL edge.

and hence a positive correlation. Similar behaviour is visible in both windows B and C, which are located downstream of window A. It is noteworthy that the negative correlation value of C_{v^*u} seems to be weakest in the intermediate window B. Moreover, the y location of this minimum value consistently shifts towards the δ_{99} line going downstream from A to C. Here, the penetration depth Δ_y is defined as the distance between δ_{99} and the location of the peak minimum in C_{v^*u}. It can be deduced that the normalized penetration depth Δ_y/δ_{99} can drop even though the physical penetration depth increases with the downstream direction since the BL grows. Note that in the DNS, since y is normalized by the reference length L, Δ_y is also normalized by L.

Figures 20(*a*,*b*) display the negative minimum value of C_{v^*u} and the penetration depth Δ_y as the reference v^* signal moves away from the wall. As expected, both these quantities diminish for all windows, i.e. as a clockwise eddy moves away from the BL edge, the induced u component inside the BL weakens, and the penetration naturally becomes shorter. In figure 20(*c*), only the reference signal at the BL edge, i.e. $y/\delta_{99} = 1$, is considered. The FST penetration depth is plotted as its true value (Δ_y), normalized by local BL thickness (Δ_y/δ_{99}) and integral length scale (Δ_y/Λ_x) versus the downstream distance. It is explicit that the true depth grows approximately 90 % from $Re_x = 0.3 \times 10^5$ to 1.6×10^5, and that it seems to scale with δ_{99}, suggesting that the penetration depth is approximately 20 % of δ_{99}. Since Λ_x grows less than δ_{99} for this FST condition, the ratio Δ_y/Λ_x grows slightly with the downstream distance. This can be an important result for future receptivity studies when the continuous FST forcing along the streamwise direction on the BL is compared with the LE receptivity.

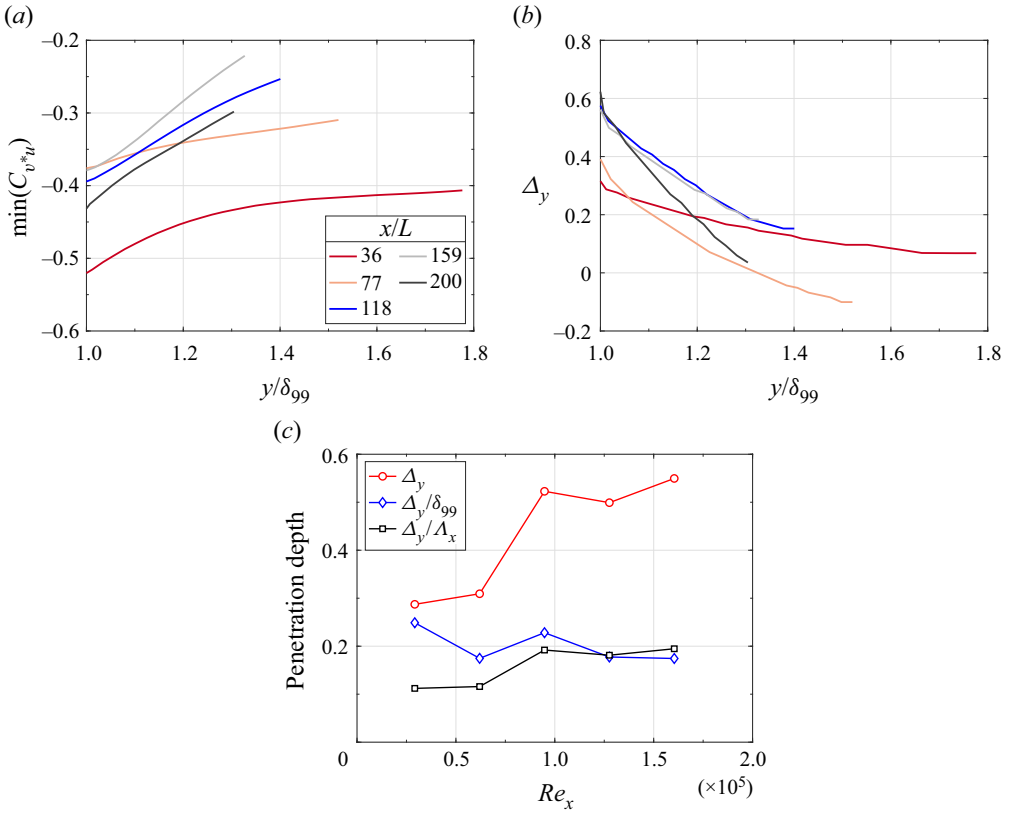

Figure 20. Minima of C_{v^*u} and Δ_y are plotted in (*a*,*b*) as a function of the reference signal location, respectively. (*c*) Downstream evolution of the penetration depth with the reference signal at the BL edge.

6. Discussion and conclusions

The influence of free-stream turbulence on a developing BL has been investigated through new experiments and available DNS data in order to deepen the common understanding of this complex transition scenario. Despite experimental imperfections, a direct and thorough comparison would, at first sight, be considered an easy task and show good agreement as long as care is taken in setting up the experiment. This is so since both experiments and DNS are considered exact methods, while CFD, making use of mathematical models, is an approximate method with results relying on how well the models really describe the complex physics. However, one should keep in mind that it is not even predictable to get good agreement between two different DNS despite being simulations of the same geometrical configuration and FST condition. The reason for this lies in: differences in applied numerical methods; inflow and description of the free-stream turbulence; LEs giving rise to different LE pressure gradients; box dimensions; grid resolution; applied boundary conditions; and so on (cf. e.g. Schlatter & Örlü (2010), where differences among DNS studies of turbulent BLs are elucidated). To the knowledge of the present authors, no one has ever made a direct comparison between two direct numerical simulations of exactly the same geometrical configuration and free-stream turbulence inflow, and very few detailed comparisons have been made between DNS and experiments, where the test cases T3A and T3B by Roach & Brierley (1992) are the most frequently

compared experiments, despite being unmeasured and therefore having unknown FST integral length scales.

However, any validation of model-based CFD results against experiments or DNS is redundant unless one can certify that detailed results fromexperiments with DNS or vice versa can be reproduced. Here, so far the most comprehensive comparison between experiments and DNS is presented in an FST induced transition scenario, a comparison that has enabled us to pinpoint the critical parameters for a satisfying comparison, here matched as well as possible. These parameters have boiled down to the following two critical factors that are essential for a fair comparison, namely:

(i) matching the external pressure gradient, particularly the pressure gradient in the LE region (to our knowledge, not necessarily the same LE geometry)
(ii) matching FST energy spectrum at the LE guaranteeing similar Tu decay and Λ_x growth.

In addition, it is important to use the same methods in analysing the data when possible, as, for instance, in calculating the intermittency factor, which is by far the most accurate measure of both the extent of the transition zone and the transition location.

In the present study, the base flows are compared through full profiles and their integral BL parameters. The comparison includes the skin-friction coefficient and the full intermittency factor distribution as well as complete wall-normal profiles of first- and second-order velocity moments. The time-averaged spanwise wavelength of the induced BL structures, i.e. the streamwise streaks, are compared as well as their amplitude growth in terms of both the maximum u^2_{rms} evolution and the wall-normal integrated counterpart. Overall, there is good agreement between the two-point cross-correlations from EXP1 to spanwise autocorrelations in DNS around the disturbance peak inside the BL. In addition, an experimental validation of the DNS simulations of Brandt *et al.* (2004) is provided, showing that small Λ_x in the free stream penetrates more easily into the BL but without leading to the fastest route to transition. This can be attributed to the fact that the FST energy spectrum does not contain enough energy in the right scales to accomplish persistent large disturbance growth inside the BL. Furthermore, full pre-multiplied PSD plots are compared in the $\mathcal{F}$–(y/δ_1) domain. It is noteworthy that this type of contour plot comparison, as shown in figure 14, is relatively common for canonical turbulent BLs. Here, one can conclude that agreement is very good between experiments and DNS with the first condition of a good match being matched transition location, which is fulfilled in this comparative study. Only then does it make sense to look into the PSD evolution for direct comparison and discuss differences. It is shown that the PSD peak evolves downstream in both $\mathcal{F}$ and (y/δ_1), and that the agreement between experiments and DNS is again very good. The overall comparison between DNS and EXP1 has to be judged very good and constitutes the first thorough direct comparison between two independent works of FST induced BL transition using different methodologies.

We elucidate and discuss the sensitivity of the BL receptivity to both (1) various LE pressure gradients, and (2) FST LE conditions. For (1), Mamidala *et al.* (2022) have shown that the LE pressure gradient plays a decisive role in FST induced transition. The influence of the suction peak in C_p and blockage due to high flap angles causing LE separation has been addressed for the new experiments (EXP1–EXP3) during this investigation. However, in terms of new results compared to Mamidala *et al.* (2022), the added value is limited and the interested reader is referred to the doctoral thesis by Mamidala (2022) (cf. § 3.1). From that analysis, one may conclude that small variations in the LE pressure gradient can have

a dramatic effect on the transition location independent of Λ_x at the studied *Tu* level of approximately 3 %. For (2), a match of the turbulence intensity and the FST integral length scale at the LE can give very different *Tu* decays and Λ_x growth, which will affect the continuous downstream FST forcing on the BL edge. For the selected showcases (EXP1 and EXP4) with seemingly similar LE FST conditions, i.e. both cases with $Tu \approx 3\,\%$ and $\Lambda_x \approx 5\,\text{mm}$, the transitional Reynolds number differs by 175 %. It is noteworthy that no firm conclusion can be made about whether it is (1) the continuous FST forcing along the BL, or (2) the fact that the FST energy spectrum at the LE does not contain enough energy in the right scales, that is most important for how disturbances grow inside the BL. Unfortunately, it seems impossible to isolate these two effects from each other in an experiment that would be required to answer this question. On the one hand, when comparing the energy spectra of EXP1 and EXP4, it is tempting to conclude that the right scales needed for an optimal disturbance growth that leads to the fastest transition, though not necessarily coinciding with the largest initial disturbance growth, are large scales of low-frequency energy. On the other hand, Fransson & Shahinfar (2020) showed that the transition location can both advance and be postponed with increasing Λ_x, and associated this behaviour to scale-matching where the actual thickness of the BL plays a decisive role for a given FST condition. With this in mind, it is likely that it is neither the large scales nor the small scales in the FST that are most important for the transition. Instead, it can be a middle-range band of frequencies that is most important, but that will vary depending on the free-stream speed, which is responsible for the BL scale. To get closer to an answer for the above effects, one needs to investigate the correlation between FST scales and the scales inside the BL.

From the DNS data, an FST penetration depth measure is defined based on the two-point cross-correlation coefficient of the streamwise velocity disturbance signal, with the reference signal being the wall-normal disturbance velocity signal in the free stream. This new measure shows that the penetration depth along the BL edge is approximately 20 % of the BL thickness up to the onset of transition, from where the measure becomes inappropriate due to the birth of turbulent spots. This is the first measure of the penetration depth, which really indicates that the FST penetration depth along the streamwise direction grows at approximately the same rate as the BL. The result is not seen as surprising, though, considering that the FST integral length scale grows, just as the BL, with the square root of the downstream distance (at least for a fully homogeneous and isotropic FST). With this result, the significance of the continuous FST forcing cannot be ruled out for the FST transition process, as has been indicated in previous studies (cf. § 1).

The present experiments–DNS comparison is satisfactory, and one can conclude that a detailed comparison of the FST transition scenario is feasible despite the higher sensitivity of a BL instability and transition experiment, compared to a fully turbulent BL experiment, due to strong energy gradients. It is concluded that the *Tu* decay could be an important feature of the FST transition process, which in that case would need to be considered in improved transition prediction models. In future experiments, it is desired to clarify how the FST penetration depth correlates with Λ_x and try to compare its importance as part of the continuous FST forcing along the downstream evolution of the BL with respect to the LE receptivity process.

Declaration of interests. The authors report no conflict of interest.

Author ORCIDs.
Santhosh B. Mamidala https://orcid.org/0000-0003-2186-9277;

André Weingärtner https://orcid.org/0000-0002-8665-2995;
Jens H.M. Fransson https://orcid.org/0000-0002-3251-8328.

References

Andersson, P., Berggren, M. & Henningson, D.S. 1999 Optimal disturbances and bypass transition in boundary layers. *Phys. Fluids* **11**, 134–150.
Antonia, R.A. & Bradshaw, P. 1971 Conditional sampling of turbulent shear flows. *Imperial College Aero. Rept.* 71-04.
Arnal, D. & Juillen, J.C. 1978 Contribution expérimentale à l'étude de la réceptivité d'une couche limite laminaire à la turbulence de l'écoulement général. *Tech. Rep.* ONERA Rapport Technique 1/5018.
Balamurugan, G. & Mandal, A.C. 2017 Experiments on localized secondary instability in bypass boundary layer transition. *J. Fluid Mech.* **817**, 217–263.
Bertolotti, F.P. 1997 Response of the Blasius boundary layer to free-stream vorticity. *Phys. Fluids* **9** (8), 2286–2299.
Brandt, L., Schlatter, P. & Henningson, D.S. 2004 Transition in boundary layers subject to free-stream turbulence. *J. Fluid Mech.* **517**, 167–198.
Brinkerhoff, J.R. & Yaras, M.I. 2015 Numerical investigation of transition in a boundary layer subjected to favourable and adverse streamwise pressure gradients and elevated free stream turbulence. *J. Fluid Mech.* **781**, 52–86.
Charnay, G., Mathieu, J. & Comte-Bellot, G. 1976 Response of a turbulent boundary layer to random fluctuations in the external stream. *Phys. Fluids* **19**, 1261–1272.
Dhawan, S. & Narasimha, R. 1957 Some properties of boundary layer flow during the transition from laminar to turbulent motion. *J. Fluid Mech.* **3**, 418–436.
Durbin, P.A. 2017 Perspectives on the phenomenology and modeling of boundary layer transition. *Flow Turbul. Combust.* **99**, 1–23.
Durovic, K. 2022 Direct numerical simulation of boundary-layer transition with free-stream turbulence. PhD thesis, KTH Royal Institute of Technology, Stockholm, TRITA-SCI-FOU, 2021:56.
Dyban, Y.E.P., Epik, E.Y.A. & Suprun, T.T. 1976 Characteristics of the laminar boundary layer in the presence of elevated free-stream turbulence. *Fluid Mech. - Sov. Res.* **5** (4), 30–36.
Ellingsen, T. & Palm, E. 1975 Stability of linear flow. *Phys. Fluids* **18**, 487–488.
Fransson, J.H.M., Matsubara, M. & Alfredsson, P.H. 2005 Transition induced by free-stream turbulence. *J. Fluid Mech.* **527**, 1–25.
Fransson, J.H.M. & Shahinfar, S. 2020 On the effect of free-stream turbulence on boundary-layer transition. *J. Fluid Mech.* **899**, A23.
Grosch, C.E. & Salwen, H. 1978 The continuous spectrum of the Orr–Sommerfeld equation. Part 1. The spectrum and the eigenfunctions. *J. Fluid Mech.* **87** (1), 33–54.
Hancock, P.E. & Bradshaw, P. 1989 Turbulence structure of a boundary layer beneath a turbulent free stream. *J. Fluid Mech.* **205**, 45–76.
Hedley, T.B. & Keffer, J.F. 1974 Turbulent/non-turbulent decisions in an intermittent flow. *J. Fluid Mech.* **64** (4), 625–644.
Hernon, D., Walsh, E.J. & McEligot, D.M. 2007 Experimental investigation into the routes to bypass transition and the shear-sheltering phenomenon. *J. Fluid Mech.* **591**, 461–479.
Hinze, J.O. 1987 *Turbulence*. McGraw-Hill.
Hislop, G.S. 1940 The transition of a laminar boundary layer in a wind tunnel. PhD thesis, Department of Engineering, King's College, University of Cambridge, UK.
Hultgren, L.S. & Gustavsson, L.H. 1981 Algebraic growth of disturbances in a laminar boundary layer. *Phys. Fluids* **24** (6), 1000–1004.
Hunt, J.C.R. & Durbin, P.A. 1999 Perturbed vortical layers and shear sheltering. *Fluid Dyn. Res.* **24**, 375–404.
Jacobs, R.G. 2000 Bypass transition phenomena studied by computer simulation. PhD thesis, Stanford University.
Jacobs, R.G. & Durbin, P.A. 1998 Shear sheltering and the continuous spectrum of the Orr–Sommerfeld equation. *Phys. Fluids* **10**, 2006–2011.
Jacobs, R.G. & Durbin, P.A. 2001 Simulations of bypass transition. *J. Fluid Mech.* **428**, 185–212.
JHTDB 2021*a* Transitional boundary layer dataset description. https://doi.org/10.7281/T17S7KX8.
JHTDB 2021*b* Webpage. http://turbulence.pha.jhu.edu, Seen: 2021-09-30.

JOHNSON, M.W. & ERCAN, A.H. 1999 A physical model for bypass transition. *Intl J. Heat Fluid Flow* **20** (2), 95–104.

JOHNSON, M.W. & FASHIFAR, A. 1994 Statistical properties of turbulent bursts in transitional boundary layers. *Intl J. Heat Fluid Flow* **15**, 283–290.

JONÁŠ, P., MAZUR, O. & URUBA, V. 2000 On the receptivity of the by-pass transition to the length scale of the outer stream turbulence. *Eur. J. Mech. (B/Fluids)* **19** (5), 707–722.

KALFAS, A.I. 1994 Transition to turbulence in the boundary layer of turbomachinery blading. PhD thesis, Cranfield University.

KENDALL, J. 1985 Experimental study of disturbances produced in a pre-transitional laminar boundary layer by weak freestream turbulence. *AIAA Paper* 85-1695.

KENDALL, J.M. 1998 Experiments on boundary layer receptivity to free-stream turbulence. *AIAA Paper* 98-0530.

KLEBANOFF, P.S. 1971 Effect of free-stream turbulence on a laminar boundary layer. *Bull. Am. Phys. Soc.* **10** (11), 1323.

KLINGMANN, B.G.B., BOIKO, A.V., WESTIN, K.J.A., KOZLOV, V.V. & ALFREDSSON, P.H. 1993 Experiments on the stability of Tollmien–Schlichting waves. *Eur. J. Mech. (B/Fluids)* **12** (4), 493–514.

KOSORYGIN, V.S. & POLYAKOV, N.P. 1990 Laminar boundary layers in turbulent flows. In *Laminar–Turbulent Transition* (ed. D. Arnal & R. Michell), pp. 573–578. Springer.

KURIAN, T. & FRANSSON, J.H.M. 2009 Grid-generated turbulence revisited. *Fluid Dyn. Res.* **41** (2), 021403.

LANDAHL, M.T. 1980 A note on an algebraic instability of inviscid parallel shear flows. *J. Fluid Mech.* **98** (2), 243–251.

LINDGREN, B. & JOHANSSON, A.V. 2002 Evaluation of the flow quality in the MTL wind-tunnel. *Tech. Rep.* KTH/MEK/TR-02/13-SE. KTH Royal Institute of Technology, Stockholm.

LUCHINI, P. 2000 Reynolds-number-independent instability of the boundary layer over a flat surface: optimal perturbations. *J. Fluid Mech.* **404**, 289–309.

MAMIDALA, S.B. 2022 Effects of free-stream turbulence and three-dimensional roughness on boundary layer transition. PhD thesis, KTH Royal Institute of Technology, Stockholm, TRITA-SCI-FOU, 2022:18.

MAMIDALA, S.B., WEINGÄRTNER, A. & FRANSSON, J.H.M. 2022 Leading-edge pressure gradient effect on boundary layer receptivity to free-stream turbulence. *J. Fluid Mech.* **935**, A30.

MASLOWE, S.A. & SPITERI, R.J. 2001 The continuous spectrum for a boundary layer in a streamwise pressure gradient. *Phys. Fluids* **13**, 1294–1299.

MATSUBARA, M. & ALFREDSSON, P.H. 2001 Disturbance growth in boundary layers subjected to free-stream turbulence. *J. Fluid Mech.* **430**, 149–153.

MUCK, K.C. 1980 Comparison of various schemes for the generation of the turbulent intermittency function. *Imperial College Aero. Rept.* 80-03.

NARASIMHA, R. 1957 On the distribution of intermittency in the transition region of a boundary layer. *J. Aero. Sci.* **24**, 711–712.

NOLAN, K.P. & WALSH, E.J. 2012 Particle image velocimetry measurements of a transitional boundary layer under free stream turbulence. *J. Fluid Mech.* **702**, 215–238.

ÖSTERLUND, J.M., JOHANSSON, A.V., NAGIB, H.M. & HITES, M.H. 1999 Wall shear stress measurements in high Reynolds number boundary layers from two facilities. *AIAA Paper* 99-3814.

OVCHINNIKOV, V., CHOUDHARI, M. & PIOMELLI, U. 2008 Numerical simulations of boundary-layer bypass transition due to high-amplitude free-stream turbulence. *J. Fluid Mech.* **613**, 135–169.

ROACH, P.E. & BRIERLEY, D.H. 1992 The influence of a turbulent free-stream on zero pressure gradient transitional boundary layer development part I: Test cases T3A and T3B. In *Numerical Simulation of Unsteady Flows and Transition to Turbulence* (ed. O. Pironneau, W. Rodi, I.L. Ryhming, A.M. Savill & T.V. Truong), pp. 319–347. Cambridge University Press.

SAVILL, A.M. 1993 Evaluating turbulence model predictions of transition. In *Advances in Turbulence IV* (ed. F.T.M. Nieuwstadt), pp. 555–562. Kluwer Academic Publishers.

SCHLATTER, P. & ÖRLÜ, R. 2010 Assessment of direct numerical simulation data of turbulent boundary layers. *J. Fluid Mech.* **659**, 116–126.

SHARP, N.S., NEUSCAMMAN, S. & WARHAFT, Z. 2009 Effects of large-scale free stream turbulence on a turbulent boundary layer. *Phys. Fluids* **21**, 095105.

STEELANT, J. & DICK, E. 2001 Modeling of laminar–turbulent transition for high freestream turbulence. *Trans. ASME J. Fluids Engng* **123** (1), 22–30.

TAYLOR, G.I. 1939 Some recent developments in the study of turbulence. In *Proceedings of the Fifth International Congress for Applied Mechanics* (ed. J. P. Den Hartog, & Peters, H.), pp. 294–310. Chapman and Hall, Ltd., London.

THOLE, K.A. & BOGARD, D.G. 1996 High freestream turbulence effects on turbulent boundary layers. *Trans. ASME J. Fluids Engng* **118**, 276–284.

WANG, B., MAO, X. & ZAKI, T.A. 2019 Low-frequency selectivity in flat-plate boundary layer with elliptic leading edge. *J. Fluid Mech.* **866**, 239–262.

WESTIN, J. 1997 Laminar–turbulent boundary layer transition influenced by free stream turbulence. PhD thesis, Department of Mechanics, Royal Institute of Technology, Stockholm, Sweden.

WESTIN, K.J.A., BOIKO, A.V., KLINGMANN, B.G.B., KOZLOV, V.V. & ALFREDSSON, P.H. 1994 Experiments in a boundary layer subjected to free stream turbulence. Part 1. Boundary layer structure and receptivity. *J. Fluid Mech.* **281**, 193–218.

WU, X., MOIN, P., WALLACE, J.M., SKARDA, J., LOZANO-DURÁN, A. & HICKEY, J.P. 2017 Transitional–turbulent spots and turbulent–turbulent spots in boundary layers. *Proc. Natl Acad. Sci. USA* **114** (27), E5292–E5299.

YOSHIOKA, S., FRANSSON, J.H.M. & ALFREDSSON, P.H. 2004 Free stream turbulence induced disturbances in boundary layers with wall suction. *Phys. Fluids* **16** (10), 3530–3539.

ZAKI, T.A. 2013 From streaks to spots and on to turbulence: exploring the dynamics of boundary layer transition. *Flow Turbul. Combust.* **91** (3), 451–473.

ZAKI, T.A. & DURBIN, P.A. 2005 Mode interaction and the bypass route to transition. *J. Fluid Mech.* **531**, 85–111.

ZAKI, T.A. & SAHA, S. 2009 On shear sheltering and the structure of vortical modes in single- and two-fluid boundary layers. *J. Fluid Mech.* **626**, 111–147.